

## Review

# Advances in Structure and Property Optimizations of Battery Electrode Materials

Jiashen Meng,<sup>1,5</sup> Haichang Guo,<sup>1,5</sup> Chaojiang Niu,<sup>1</sup> Yunlong Zhao,<sup>3</sup> Lin Xu,<sup>1,4,\*</sup> Qi Li,<sup>1</sup> and Liqiang Mai<sup>1,2,\*</sup>

**Rechargeable batteries undoubtedly represent one of the best candidates for chemical energy storage, where the intrinsic structures of electrode materials play a crucial role in understanding battery chemistry and improving battery performance. This review emphasizes the advances in structure and property optimizations of battery electrode materials for high-efficiency energy storage. The underlying battery reaction mechanisms of insertion-, conversion-, and alloying-type materials are first discussed toward rational battery designs. We then give a summary of the advanced optimization strategies and provide in-depth analyses of structure-property relationships for some significant research breakthroughs in batteries. Finally, we provide a brief overview of the recent state-of-the-art techniques as powerful tools to explore and predict the strategies of structure optimization. This review on the deep understanding of structure-property correlations will bring new insight into the design of ideal battery materials and open up new opportunities for battery chemistry.**

## Introduction

In the past decades, traditional non-renewable energy supplies (e.g., coals, oil, natural gas) have been overused to meet the rapid increase of global energy demands, leading to the emergency problems of climate change, smog, and impending exhaustion of fossils fuels.<sup>1,2</sup> In this regard, more and more renewable green energy technologies (especially solar and wind energy) are being urgently explored. To utilize these intermittent renewable energies efficiently, developing low-cost and high-performance electrical energy storage techniques is the key.<sup>3</sup> Meanwhile, with the economy fast booming, there is also an increasing market demand for smaller and lighter portable electronics and smart electric vehicles with high power/energy density and long lifespan.<sup>4</sup> All of these demands call for intensive efforts to develop highly efficient and environmentally benign energy storage devices.

Rechargeable batteries that are able to efficiently convert chemical energy to electrical energy rely on electrochemical processes to store energy.<sup>2</sup> Among all rechargeable batteries, lithium-ion batteries (LIBs) have achieved the dominant position for chemical energy storage because of slow self-discharge, long cycle life, no memory effect, and relatively high energy/power densities.<sup>5</sup> These superior characteristics enable LIBs to be widely applied on portable electronics and emerging electrical/hybrid vehicles. Free from lithium metal, LIBs involve the reversible shuttling processes of lithium ions between host anode and cathode materials with concomitant redox reactions during the charge/discharge processes.<sup>6</sup>

## Context & Scale

Increasing energy demands for potential portable electronics, electric vehicles, and smart power grids have stimulated intensive efforts to develop highly efficient rechargeable batteries for chemical energy storage. The intrinsic structures of electrode materials are crucial in understanding battery chemistry and improving battery performance for large-scale applications. This review presents a new insight by summarizing the advances in structure and property optimizations of battery electrode materials for high-efficiency energy storage. In-depth understanding, efficient optimization strategies, and advanced techniques on electrode materials are also highlighted.

By now, many challenges still exist for achieving great breakthroughs in high-performance scalable batteries. To address the challenges, some important aspects are proposed on the development of battery research in the future. First, it is highly desired to develop new electrode materials and new storage devices to meet the urgent energy demands for large-scale

Sodium-ion batteries (SIBs), as another type of electrochemical energy storage device, have also been investigated for large-scale grid energy storages due to low cost and abundant source of sodium as well as its similar physicochemical properties to lithium.<sup>7</sup> To meet the challenges of high energy/power density, low cost, good safety, and long lifespan for batteries in the near future, developing novel electrode materials is essential.

By now, a significant amount of battery research for both fundamental studies and practical applications has been conducted. Intensive efforts have been dedicated to developing various methods to improve the battery performance via nanotechnology.<sup>8</sup> These methods mainly focus on the surface engineering achieved by downsizing particles, facet engineering, and structural engineering (e.g., designing complex multilevel structures).<sup>9,10</sup> For instance, because the commercial olivine orthophosphate lithium iron(II) phosphate LiFePO<sub>4</sub> suffers from the low electronic conductivity and only one-dimensional (1D) [010] diffusion channel, both the size and orientation control of LiFePO<sub>4</sub> are necessary.<sup>11–13</sup> Zhao et al. reported the preparation of single crystalline LiFePO<sub>4</sub> nanosheets with a large percentage of highly oriented (010) facets, which provided the highest pore density and shortest diffusion length for lithium-ion insertion/extraction.<sup>13</sup> This architecture exhibited impressive rate capability and excellent cycling stability in LIB. In addition, various carbon-based nanostructured composites with delicate designs have been developed, which exhibited outstanding electrochemical properties due to the improvement in the electronic conductivity and strong mechanical stability.<sup>14,15</sup> Compared with commercial graphite, silicon has attracted significant attention as a potential anode material because of its relatively abundant source and high theoretical specific capacity ( $\sim 4,200 \text{ mAh g}^{-1}$ ). However, some issues such as large volume variation and unstable solid-electrolyte interphase (SEI) during the charge/discharge processes are limiting its further applications. To address these scientific problems, Cui's group designed and constructed silicon nanowire array, self-healing silicon microparticles, silicon/graphite composites, and silicon pomegranates, which have efficiently improved the electrochemical performance.<sup>16–19</sup> These nanotechnology-based approaches toward the design and fabrication of functional electrode materials endow batteries with high energy/power densities and long-term cyclability.<sup>20</sup> Unfortunately, the hollow interiors and delicate architectures lead to low packing density and high preparation cost, hence restricting their practical applications.

Many challenges still exist for achieving great breakthroughs in high-performance batteries for large-scale applications.<sup>7,21,22</sup> Compared with nanotechnology-based designs, the intrinsic phase structures of electrode materials play a more crucial role in lifting battery performance and understanding the battery reaction chemistry. Clearly, the electrochemical properties of these electrode materials (e.g., voltage, capacity, rate performance, cycling stability, etc.) are strongly dependent on the correlation between the host chemistry and structure, the ion diffusion mechanisms, and phase transformations.<sup>23</sup>

In this review, we provide a summary on the advances in the purview of structure and property optimizations of battery electrode materials for high-efficiency energy storage. Particular emphasis is first placed on deep understanding of the underlying battery reaction mechanisms of insertion-, conversion-, and alloying-type materials toward rational design of batteries. Second, we review the optimization strategies and conduct in-depth analyses of crystal structures for some significant research breakthroughs on high-performance batteries. For each type of electrode material, some promising optimization strategies are discussed to solve the corresponding

applications. Second, the in-depth understanding of the fundamental reaction mechanisms and the structure-property correlations is essential. Third, it is critical to explore low-cost electrode materials and fabrication processes for large-scale applications in industry. Moreover, bridging the fundamental research in laboratory and the scalable development in industry is extremely important in directing lab-based research toward practical applications.

Based on the in-depth understanding of battery chemistry in electrode materials, some important reaction mechanisms and design principles are clearly revealed, and the strategies for structure optimizations toward high-performance batteries are summarized. This review will provide a suitable pathway toward the rational design of ideal battery materials for large-scale applications in industry and open up new opportunities for battery chemistry.

<sup>1</sup>State Key Laboratory of Advanced Technology for Materials Synthesis and Processing, Wuhan University of Technology, Wuhan 430070, China

<sup>2</sup>Department of Chemistry, University of California, Berkeley, CA 94720, USA

<sup>3</sup>Department of Chemistry and Chemical Biology, Harvard University, Cambridge, MA 02138, USA

<sup>4</sup>School of Chemical and Biomedical Engineering, Nanyang Technological University, 62 Nanyang Drive, Singapore 637459, Singapore

<sup>5</sup>These authors contributed equally

\*Correspondence: xu.lin@ntu.edu.sg (L.X.), mlq518@whut.edu.cn (L.M.)

<https://doi.org/10.1016/j.joule.2017.08.001>

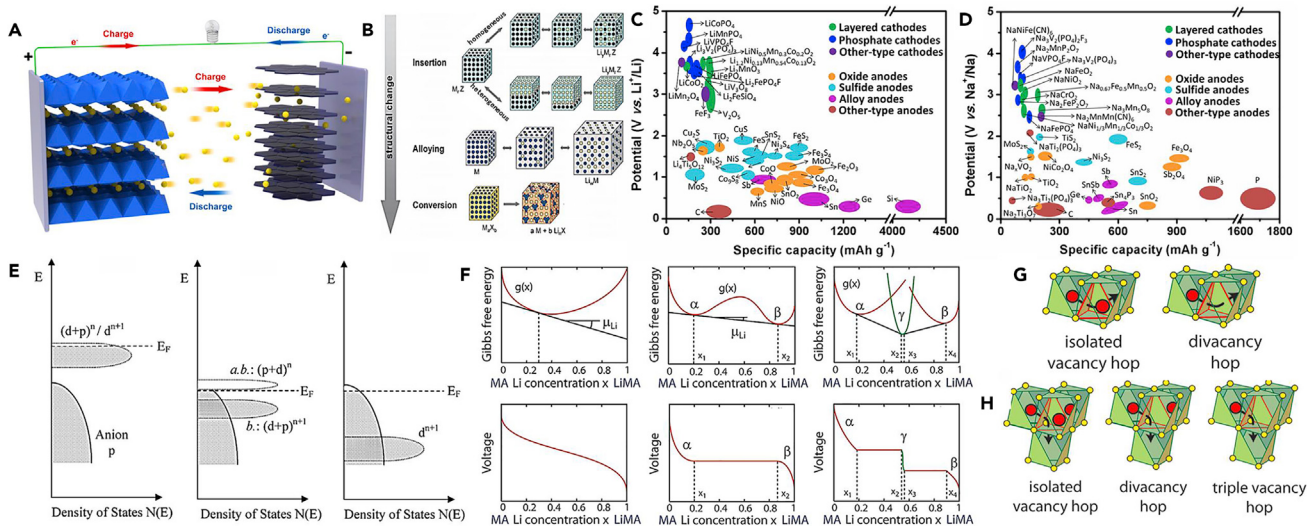


**Figure 1. In-Depth Understanding of Battery Chemistry of Electrode Materials**

- (A) Schematic of a first-generation rechargeable LIB. This LIB involves reversible shuttling processes of lithium ions between two host anode (graphite) and cathode (LiCoO<sub>2</sub>) materials with concomitant redox reaction during the charge/discharge processes.
- (B) Schematic of three different reaction mechanisms in electrode materials for batteries. Reprinted with permission from Palacín et al.<sup>25</sup> Copyright 2009, Royal Society of Chemistry.
- (C and D) Operation voltages versus specific capacities of LIB (C) and SIB (D) electrode materials, respectively.
- (E) Schematic of a slightly oxidized redox couple for different positions relative to the top of the anion p bands. Reprinted with permission from Goodenough et al.<sup>22</sup> Copyright 2010, American Chemical Society.
- (F) Voltage curves that are linearly related to the slope of the free energy of the electrode materials.
- (G and H) Diffusion paths in layered (G) and spinel (H) crystal structures mediated by vacancy clusters, respectively. Reprinted with permission from Van der Ven et al.<sup>26</sup> Copyright 2013, American Chemical Society.

critical scientific problems. Third, we also present recent advanced techniques that have emerged to become powerful tools to investigate and predict optimization strategies, including micro-/nanoscale electrochemical devices, high-resolution characterizations, and theoretical calculations. Finally, the remaining challenges and the outlook of future battery research are discussed. This review may open new avenues for the design of ideal electrode materials and bring new opportunities for future battery research.

## Understanding Electrode Materials toward Rational Design of High-Performance Batteries

Batteries are electrochemical devices that store energy by chemical reactions. The structure of a typical first-generation LIB, which includes a cathode, an anode, electrolyte, separator, and external circuit, is shown in Figure 1A.<sup>24</sup> During charging, lithium ions are extracted from the LiCoO<sub>2</sub> crystal driven by an applied voltage, followed by diffusing through the electrolyte and then being intercalated between graphite sheets. During discharging, the directions are reversed along with generated power to external devices. To acquire high-performance batteries, it is important to understand the ion/electron transport and reaction mechanisms in electrode materials.<sup>21</sup> In this section, we first describe three types of electrode materials according to their reaction mechanisms. The thermodynamic and kinetic analyses are then discussed to obtain an in-depth understanding of the structure-property relationships of the electrode materials. Finally, three design principles for the electrode materials are proposed from the structural aspects, which reveal the basic rules of the structure optimization strategies.

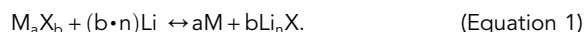
### Different Types and Challenges of Electrode Materials

According to the reaction mechanisms of electrode materials, the materials can be divided into three types: insertion-, conversion-, and alloying-type materials (Figure 1B).<sup>25</sup> The voltages and capacities of representative LIB and SIB electrode materials are summarized in Figures 1C and 1D.

Insertion-type materials involve the insertion process of lithium (or, e.g., sodium) ions into the interstitial sites of the electrode materials and the subsequent process to capture electrons. Most insertion-type materials have robust crystalline skeletons and are easy for ion insertion and removal, which endows them with long-term cycling stability and high rate capability. These characteristics allow them to have excellent stability and good safety and hence to be widely used in commercial batteries. In the past decades, intensive efforts have been made to develop various insertion-type materials. Generally, according to the crystalline structure, insertion-type materials can be categorized into two major groups: layered oxides (e.g., LiCoO<sub>2</sub>, LiV<sub>3</sub>O<sub>8</sub>, V<sub>2</sub>O<sub>5</sub>, LiNi<sub>x</sub>Co<sub>1-x-y</sub>Al<sub>y</sub>O<sub>2</sub>, LiNi<sub>x</sub>Co<sub>1-x-y</sub>Mn<sub>y</sub>O<sub>2</sub>, Li<sub>2</sub>MnO<sub>3</sub>, and Li<sub>1.2</sub>Ni<sub>0.13</sub>Mn<sub>0.54</sub>Co<sub>0.13</sub>O<sub>2</sub>) and polyanionic compounds (e.g., PO<sub>4</sub><sup>3-</sup>, SO<sub>4</sub><sup>2-</sup>, SiO<sub>4</sub><sup>4-</sup>, BO<sub>3</sub><sup>3-</sup>, and fluoride-containing PO<sub>4</sub><sup>3-</sup>).<sup>27</sup> However, most of insertion-type materials have a relatively low specific capacity because of their limited interstitial sites. In addition, some high-capacity cathode materials (e.g., Li<sub>2</sub>FeSiO<sub>4</sub>, Li<sub>2</sub>MnSiO<sub>4</sub>, Li<sub>2</sub>MnO<sub>3</sub>, and Li<sub>1.2</sub>Ni<sub>0.13</sub>Mn<sub>0.54</sub>Co<sub>0.13</sub>O<sub>2</sub>) suffer from serious structural transformations during cycling, leading to large initial irreversible capacity and poor cycling stability.

Alloying-type materials mainly refer to some metal or metalloid materials that can form alloy with lithium or sodium, among others.<sup>28</sup> A typical reaction mechanism is illustrated in Figure 1B. Compared with the insertion-type materials, these materials can offer much larger specific capacity. Materials that undergo an alloying process include Si, Sn, In, Bi, Zn, Te, and intermetallic compounds. However, in the host structures the large volume change upon the ion insertion and extraction is a major and catastrophic problem for further practical applications of alloying-type materials.<sup>29</sup> During charging, electrochemical reduction of the electrolyte occurs and thereby forms a passivating and insulated SEI film. The large volume variation of the alloying materials can easily lead to the thickening and destabilization of the SEI film, hence resulting in low coulombic efficiency and rapid capacity decay. In addition, the lithium metal anode suffers from similar aforementioned problems. For this reason the optimization strategies for lithium metal are discussed in the same section as alloying-type materials.

Since 2000, when Tarascon et al. first reported using transition metal oxides as LIB anode materials, conversion-type materials have been widely studied.<sup>30</sup> For LIBs, a typical chemical equation of conversion-type materials is



Here M represents the transition metal elements such as Fe, Co, Ni, Cu, etc.; X represents O, S, N, P, F, and H elements; and n is the valence number of X. Compared with other types of materials, a characteristic feature of the conversion-type materials is the formation of at least two products. The reduction of M<sub>a</sub>X<sub>b</sub> into metallic state is often a multi-electron reaction, which endows conversion-type materials with a high capacity.<sup>29</sup> However, large volume change, low conductivity, and severe voltage hysteresis have limited their applications.

As chemical devices, understanding of the electrode surface chemistry in LIBs is also necessary. Generally a passivating layer called the SEI is formed on the

negative and positive electrodes of LIBs as a result of electrolyte decomposition, mainly during the first cycle.<sup>20</sup> The SEI is a lithium-ion conductor but an electronic insulator, which mainly consists of polycrystalline materials. The electrolyte solution is thermodynamically unstable at low and very high potentials versus Li<sup>+</sup>/Li. For a negative electrode, the formation of SEI, which consists of inorganic Li<sub>2</sub>O, Li<sub>2</sub>CO<sub>3</sub>, or LiOH, is attributed to the working potential below the chemical composition of the SEI on reduction potential of electrolytes.<sup>31</sup> By contrast, the chemical composition of the SEI formed on commercial graphite is generally similar to that formed on metallic lithium. However, the variety of morphologies can cause compositional differences of the SEI, and solvent co-intercalation also occurs along with lithium intercalation, leading to exfoliation of the graphite electrode. For a positive electrode, electrolyte oxidation is a major cause of SEI formation. Different from negative electrode, the SEI on positive electrode is mainly composed of organic species (e.g., polymer/polycarbonate).<sup>32</sup> In brief, the stable SEI on electrodes has significant influence on the safety, power capability, shelf life, and cycle life of the battery.

#### Deep Understanding of Battery Reaction Mechanisms

##### Thermodynamic Analysis

**Fermi Energy Level Perspective.** In the band structure, Fermi energy level refers to a hypothetical energy level of an electron where the electron occupation probability equals 0.5 at the thermodynamic equilibrium.<sup>33</sup> In fact, the Fermi energy level is the driving force of electron transport, enabling the electrons to migrate from the negative electrode with a high energy level to the positive electrode with a low-energy level during discharge.<sup>33</sup>

For insertion-type materials, the change in Fermi energy level of the transition metal ions influences the charge/discharge reversibility of a battery. The electronic structure of transition metal ions is 3d4s, so the loss or gain of 3d-electrons corresponds to the oxidation or reduction of transition metal elements during the charge/discharge processes. Usually electrons which hop into insertion-type materials can be seen as "small polarons," which cause the phase interface migration.<sup>33</sup> Therefore, some reaction mechanisms in electrode materials, such as two-phase reaction or solid-solution reaction, can be explained accordingly.

In material design, it is necessary to match the energy level of the redox couple of a transition metal with the p-orbital of the anion (Figure 1E).<sup>22</sup> Usually, the Fermi energy level can vary from  $(d + p)^n/d^{n+1}$  to the bottom of the combinational bonding  $(p + d)^n$ , and even into the anion's p band. When Fermi energy level is at the anion's p band, the gain or loss of anions' electrons will directly cause the structural instability. The position of the p-orbital energy level restricts the voltage of the electrode materials intrinsically.<sup>33</sup> In fact, since oxygen has a lower energy level with a 2p-orbital than sulfur with a 3p-orbital, oxide cathodes are much more widely applied than sulfide ones.<sup>22</sup> Furthermore, the match of Fermi energy level with the lowest unoccupied molecular orbital (LUMO) of electrolyte is another issue and needs to be taken into account. Since the Fermi energy levels of alloying-type and conversion-type materials are usually lower than the LUMO of organic electrolyte, the SEI film in the initial cycles is easily formed on their surfaces.<sup>33</sup>

**Gibbs Free Energy Perspective.** Different from Fermi energy level, Gibbs free energy refers to the minimized thermodynamic potential when a reaction system reaches the chemical equilibrium at a constant pressure and temperature. According

to the Nernst equation, the voltage ( $\Phi$ ) between the anode and cathode materials is expressed by the corresponding chemical potentials in the following equation<sup>26</sup>:

$$\Phi = -\frac{\mu_C - \mu_A}{F}, \quad (\text{Equation 2})$$

where F is the Faraday constant, and  $\mu_C$  and  $\mu_A$  refer to the chemical potential of cathode and anode, respectively. As illustrated in Figure 1F, the straightforward correlation between a measurable voltage curve and the Gibbs free energy means that the change of Gibbs free energy and phase transformations due to variations in Li concentration will have significant influence in the voltage profile.<sup>26</sup> Some representative transformations are clearly revealed, including the solid-solution reaction, the first-order phase-transformation, and phase-separation reaction. Therefore, Gibbs free energy affects the chemical potential and, hence, the voltage. In addition, oxygen chemical potential shows great importance in the design of high-voltage cathode materials (>4.5 V).<sup>34</sup> Usually a high voltage causes a higher oxygen chemical potential in cathode materials at the charge state. If the oxygen chemical potential is above 0 eV, O<sub>2</sub> release will occur from the crystal lattices of the charged cathode, leading to severe structural degradation and safety problems.<sup>35</sup> Therefore, the development of high-voltage cathodes with a far-negative oxygen chemical potential is crucial to powerful, stable, and safe batteries.

**Kinetic Analysis.** While thermodynamic factors determine the shape of the voltage profile and intrinsic capacity, rate properties depend on kinetic factors such as ion mobility and phase-transformation mechanisms. The chemical diffusion coefficient (D) is a basic parameter to describe the Li-ion mobility. D can be written as follows<sup>26,36</sup>:

$$D = \rho \lambda^2 \Gamma, \quad (\text{Equation 3})$$

where  $\rho$  is a geometric factor that depends on the symmetry of the sublattice of interstitial sites and  $\lambda$  is the hop distance between adjacent interstitial sites. Hop frequency ( $\Gamma$ ) can be expressed as<sup>26</sup>

$$\Gamma = v^* \exp\left(\frac{\Delta E}{kT}\right). \quad (\text{Equation 4})$$

Here,  $v^*$  is a vibrational factor and  $\Delta E$  is the migration barrier. Therefore, as D has an exponential dependence on  $\Delta E$ , a small variation in the migration barrier due to compositional, chemical, and/or crystallographic changes will be amplified to a large change in the diffusion coefficient.

In a layered structure, Li usually prefers to occupy octahedral interstitial sites in insertion-type materials and hops along a curved path through an adjacent tetrahedral site.<sup>37</sup> The energy of the intermediate state when Li goes through the tetrahedral sites determines the Li hop path. According to the vacancy cluster diffusion mechanism, the divacancy hop is easier than the isolated vacancy hop due to the absence of repulsion force vacancy hop (Figure 1F). Similarly, triple vacancy hop is the first choice in a spinel structure with respect to its three-dimensional nature (Figure 1G). The different diffusion paths have a significant influence on the chemical diffusion coefficient in the host materials.

#### Design Principles for Battery Electrode Materials

Based on the above discussions, all of the thermodynamic and kinetic analyses are aimed to establish the relationships between structure (especially crystal structure) and properties (capacity, voltage, and rate), and to provide a direction for the rational design and optimization of electrode materials toward high-performance

batteries. Some important design principles for electrode materials are considered to be able to efficiently improve the battery performance.

**Excellent Host Chemistry.** Host chemistry strongly depends on the composition and structure of the electrode materials, thus influencing the corresponding chemical reactions. According to the aforementioned discussions, Gibbs free energy (chemical potential) and Fermi energy level can be used to describe the chemical composition and the electronic structure of electrode materials, respectively, which offers a better pathway to design electrode materials with a high capacity and a high voltage. Therefore, good design of composition and structure for excellent host chemistry can create additional highly reversible redox reactions and fast chemical reaction kinetics, thus improving the properties of electrode materials.

**Efficient Ion and Electron Transport.** Efficient ion and electron transport is crucial to the electrochemical reactions of a battery. In terms of crystal structures, chemical diffusion coefficient is a key kinetic parameter to describe the Li-ion mobility, and Fermi energy level is the driving force of electron transport. Considering comprehensive thermodynamic and kinetic factors, rational design on crystal structures of new electrode materials with efficient ion and electron transports can realize a high rate capability for batteries. In addition, coating active electrode materials with a conductive layer or embedding the active electrode materials in a conductive matrix can also efficiently improve the electron conductivity of the whole electrode.

**Long-Term Structural Stability.** The structural stability of electrode materials includes two main aspects, the crystal structure and the reaction interface. Thermodynamic parameters can give us a basic prediction of the structural properties of an electrode material. For example, a low anion's p band and a more negative oxygen chemical potential at the charged state are beneficial to the overall structural stability in electrode materials. On the other hand, from the Fermi energy level, electrochemical reduction of the electrolyte generates a passivated and insulated SEI film on the surface of conversion-/alloying-type materials during charging. Owing to large volume changes on lithiation and delithiation, forming a stable SEI film is highly challenging and desirable for realizing long-term cycling performance.

### Optimization Strategies for Insertion-type Materials

In the past decades, insertion-type materials have attracted much attention as promising cathode materials for batteries. However, there some issues exist regarding these materials, such as low capacity, unsatisfactory diffusion coefficient, and structure degradation. On the basis of the aforementioned design principles, various important optimization strategies have been developed to realize the rational design of insertion-type materials for high-performance batteries, including stabilized/enlarged diffusion channel, phase control, strain accommodation, ion doping, and synergistic effect (Table 1).

#### Stabilized/Enlarged Diffusion Channel

The stabilized and enlarged diffusion channel of electrode materials is crucial for the long-term cycling performance and rate capability in batteries. However, after the long-term charge/discharge process, the structure degradation of most layered oxide cathode materials irreversibly transformed the electrode materials to an inactive state, leading to poor cycling stability and rate capability. One general method is to use the intercalation of ions into layered electrode materials to improve the cycling capability. Zhao et al. systematically investigated alkali metal ion (Li, Na, K, and Rb) intercalation compounds for LIBs.<sup>38</sup> The intercalation of appropriate alkali

**Table 1. Structure Optimization Strategies for Insertion-, Alloying-, and Conversion-type Electrode Materials**

Electrode Materials	Advantages	Challenges	Structure Optimization Strategies	Examples
Insertion-type materials	easy ion insertion and extraction robust crystalline skeletons relatively high voltage	limited insertion sites structural degradation low conductivity	stabilized/enlarged diffusion channel <sup>38–43</sup>	K-V-O expanded graphite $Zn_{0.25}V_2O_5 \cdot nH_2O$ Peo-MoS <sub>2</sub> $K_3V_2(PO_4)_3$ $Na_3V_2(PO_4)_3$
			phase control <sup>44–47</sup>	P2- $Na_{2/3}[Fe_{1/2}Mn_{1/2}]O_2$ bilayered $V_2O_5$ cation-disordered $Li_{1.211}Mo_{0.467}Cr_{0.3}O_2 Li_{1.17}Ni_{0.17}Co_{0.17}Mn_{0.5}O_2 @ Li\text{-}Mg\text{-}PO_4$
			strain accommodation <sup>48–51</sup>	P2- $Na_{0.66}[Li_{0.22}Ti_{0.78}]O_2$ $Li_2MoO_3$ LiFePO <sub>4</sub> nanoplatelets $LiNi_{0.8}Co_{0.15}Al_{0.05}O_2 @ Li_xCoO_2$
			ion doping <sup>52–59</sup>	$Na_{0.44}[Mn_{1-x}Ti_x]O_2$ $LiNi_xMn_{2-x}O_4$ Al-doped Li-/Mn-rich oxides doped LiFePO <sub>4</sub>
Alloying-/conversion-type materials	large theoretical capacity low cost abundant sources	large volume variation unstable SEI low conductivity voltage hysteresis	Phase-buffering mechanism <sup>65–69</sup>	CaFe <sub>2</sub> O <sub>4</sub> $Ca_3Co_4O_9$ $Ni_3Sn_2$ amorphous Si Fe-Cu-Si ternary composite
			continuous conductive phase control <sup>70–77</sup>	$Cu_yFe_{1-y}F_2$ conductive-gel-framework electrodes modified Li metals
			synergistic effect <sup>78–80</sup>	$ZnCo_2O_4$ $SnO_2/Fe_2O_3/Li_2O$ $SnO_2\text{-}Fe/Mn\text{-}graphite$

metal ions, acting as pillars, could enlarge the diffusion channel and stabilize the metal oxide interlayer structure (Figure 2A). After 100 cycles at 0.1 A g<sup>-1</sup>, the capacity retention of A-V-O electrodes was about 95%, much higher than that of V<sub>2</sub>O<sub>5</sub> (37.6%), indicating their excellent structural stability (Figure 2B). Figure 2C demonstrates that the A-V-O electrodes possess good rate capability. Even at a highest current density of 37 C, the capacity of the K-V-O could reach as high as ~110 mAh g<sup>-1</sup>. Recently, Kundu et al. reported a new Zn<sub>0.25</sub>V<sub>2</sub>O<sub>5</sub>·nH<sub>2</sub>O material as a cathode material for an aqueous rechargeable zinc battery (Figure 2D).<sup>39</sup> After 200 cycles, the as-prepared Zn<sub>0.25</sub>V<sub>2</sub>O<sub>5</sub>·nH<sub>2</sub>O electrode delivered a high reversible specific capacity of ~260 mAh g<sup>-1</sup> and an excellent cycling capability at 1,200 mA g<sup>-1</sup>. The superior electrochemical performance of the Zn<sub>0.25</sub>V<sub>2</sub>O<sub>5</sub>·nH<sub>2</sub>O electrode was attributed to the pillar effect of interlayered Zn<sup>2+</sup> ions and water molecules, thereby stabilizing its crystal structure and facilitating the ion transport.

Alternatively, the enlargement of the diffusion channel by adjusting the lattice parameters is also an efficient way to improve the chemical diffusion coefficient and hence enhance their electrochemical performance. An et al. reported Na<sub>3</sub>V<sub>2</sub>(PO<sub>4</sub>)<sub>3</sub>, a typical Na<sup>+</sup> ion superionic conductor (NASICON) with superior Li storage performance. Due to a smaller ionic radius of Li<sup>+</sup> (0.76 Å) than that of Na<sup>+</sup> (1.06 Å), the faster diffusion of Li<sup>+</sup> ions in Na<sub>3</sub>V<sub>2</sub>(PO<sub>4</sub>)<sub>3</sub> results in an outstanding rate performance (Figure 2E).<sup>40</sup> Recently, Liang et al. also developed a general interlayer expansion approach to synthesize MoS<sub>2</sub> with an enlarged interlayer distance by inserting a controlled amount of poly(ethylene oxide) (PEO).<sup>41</sup> By modulating the amount of PEO in MoS<sub>2</sub>, the interlayer distances can be efficiently tuned (Figures

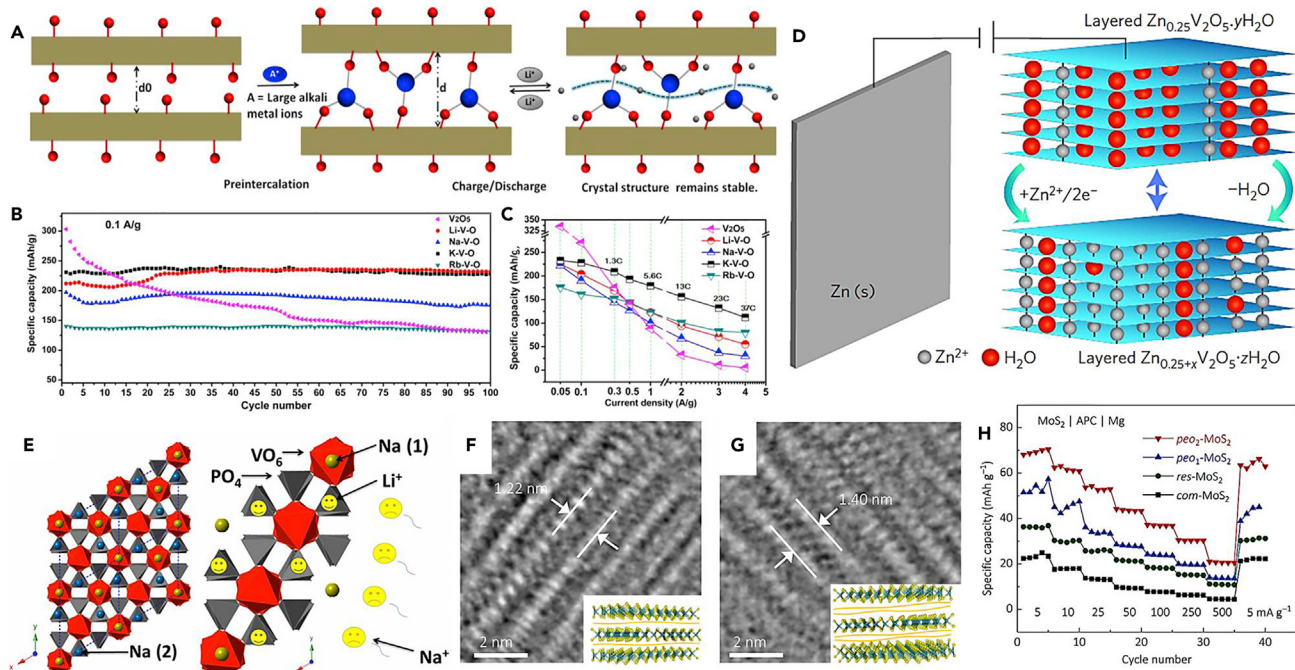


**Figure 2. Typical Examples of Battery Electrode Materials Based on Stabilized/Enlarged Diffusion Channel**

(A) Schematic of the large alkali metal ion intercalation process.

(B) Cycling performance of A-V-O nanowires formed by pre-intercalating large alkali metal into vanadium oxides at a current density of  $0.1 \text{ A g}^{-1}$ .

(C) Rate performance of A-V-O nanowires at various current densities of  $0.05\text{--}4.0 \text{ A g}^{-1}$ . Reprinted with permission from Zhao et al.<sup>38</sup> Copyright 2015, American Chemical Society.

(D) Schematic of the Zn metal/ $Zn_{0.25}V_2O_5 \cdot yH_2O$  cell on discharge in aqueous  $1 \text{ M ZnSO}_4$ . Reprinted with permission from Kundu et al.<sup>39</sup> Copyright 2016, Macmillan Publishers Limited.

(E) The crystal structure of  $Na_3V_2(PO_4)_3$  and schematic of the comparison for the diffusion of  $Li^+$  and  $Na^+$  ions in  $Na_3V_2(PO_4)_3$ . Reprinted with permission from An et al.<sup>40</sup> Copyright 2015, Wiley-VCH.

(F and G) High-resolution TEM images of  $peo_1\text{-MoS}_2$  (F) and  $peo_2\text{-MoS}_2$  (G) with different amounts of PEO in the interlayer.

(H) Rate performance for four kinds of  $\text{MoS}_2$  samples. Reprinted with permission from Liang et al.<sup>41</sup> Copyright 2015, American Chemical Society.

2F and 2G). High-resolution transmission electron microscopy (TEM) images showed that the interlayer distances of  $peo_1\text{-MoS}_2$  and  $peo_2\text{-MoS}_2$  samples were 1.22 and 1.41 nm, which were larger than those of pristine  $\text{MoS}_2$  (com- $\text{MoS}_2$ , 0.61 nm) and simply restacked  $\text{MoS}_2$  (res- $\text{MoS}_2$ , 0.62 nm). The  $peo_2\text{-MoS}_2$  sample with the largest interlayer distance exhibited superior magnesium storage, indicating the increased  $Mg^{2+}$  ion diffusion kinetics (Figure 2H). This strategy of enlarging the diffusion channel can be extended to other insertion-type materials.<sup>42,43</sup> Graphite with expanded interlayers could also possess enhanced anode performance in SIBs.<sup>43</sup>

#### Phase Control

Recently, layered oxides have become the most extensively studied topic in SIBs.<sup>7</sup> According to the occupied sites of sodium ions between the layers, there are mainly two types, O3 type (octahedral sites) and P2 type (prismatic sites). Yabuuchi et al. reported P2-type  $\text{Na}_{2/3}[\text{Fe}_{1/2}\text{Mn}_{1/2}]O_2$  and O3-type  $\text{Na}[\text{Fe}_{1/2}\text{Mn}_{1/2}]O_2$  as promising cathode materials for SIBs (Figures 3A and 3B).<sup>44</sup> The P2-type  $\text{Na}_{2/3}[\text{Fe}_{1/2}\text{Mn}_{1/2}]O_2$  electrode delivered a higher reversible discharge capacity of  $190 \text{ mAh g}^{-1}$ , a lower polarization voltage of  $<0.5 \text{ V}$ , and a higher coulombic efficiency of  $\sim 96\%$  than those of O3-type  $\text{Na}[\text{Fe}_{1/2}\text{Mn}_{1/2}]O_2$  ( $\sim 110 \text{ mAh g}^{-1}$ ,  $>1 \text{ V}$ , and  $\sim 85\%$ ). Sodium ions in P2-type layered framework migrated from one prismatic site to adjacent sites with a lower diffusion barrier, indicating that the excellent performance of P2-type

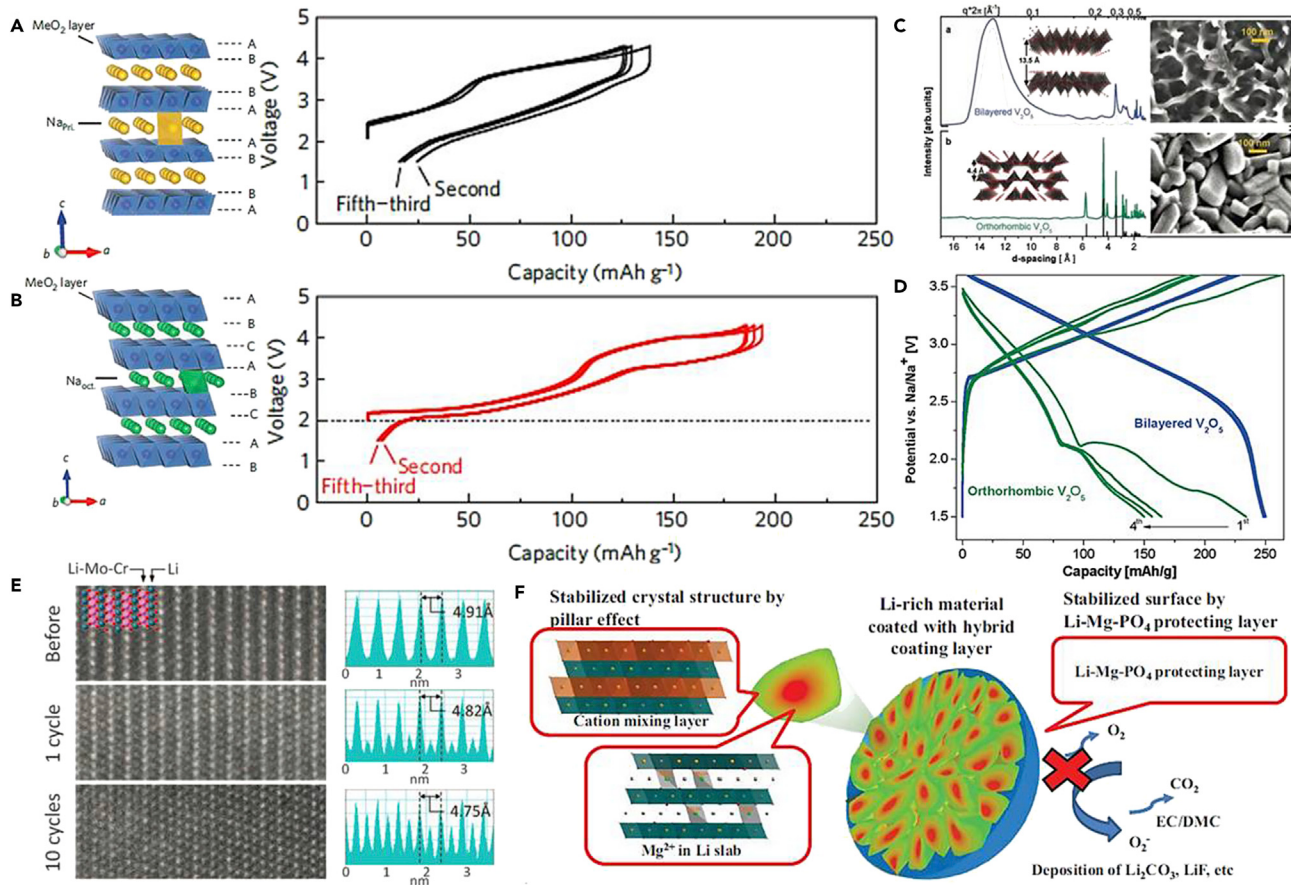


**Figure 3. Typical Examples of Battery Electrode Materials Based on Phase Control**

(A and B) Crystal structures and galvanostatic charge/discharge curves of P2-type  $\text{Na}_{2/3}[\text{Fe}_{1/2}\text{Mn}_{1/2}] \text{O}_2$  (A) and O3-type  $\text{Na}[\text{Fe}_{1/2}\text{Mn}_{1/2}] \text{O}_2$  at  $12 \text{ mA g}^{-1}$  (B) in the voltage range from 1.5 to 4.2 V versus  $\text{Na}^+/\text{Na}$ , respectively. Reprinted with permission from Yabuuchi et al.<sup>44</sup> Copyright 2012, Macmillan Publishers Limited.

(C) Synchrotron XRD patterns, scanning EM images, and crystal simulations of bilayered  $\text{V}_2\text{O}_5$  and orthorhombic  $\text{V}_2\text{O}_5$ , respectively.

(D) The corresponding charge/discharge curves in SIBs. Reprinted with permission from Tepavcevic et al.<sup>45</sup> Copyright 2011, American Chemical Society.

(E) STEM images and corresponding line profiles along the [010] zone axis in an LMCO/C particle before cycling and after 1 and 10 cycles (1.5–4.3 V, C/20). Reprinted with permission from Lee et al.<sup>46</sup> Copyright 2014, American Association for the Advancement of Science.

(F) Schematic of Li-rich cathode material particle with the stabilization effect by novel surface phase control. Reprinted with permission from Liu et al.<sup>47</sup> Copyright 2015, Wiley-VCH.

$\text{Na}_{2/3}[\text{Fe}_{1/2}\text{Mn}_{1/2}] \text{O}_2$  is attributed to the intrinsic phase structure.<sup>7</sup> Tepavcevic et al. developed an electrochemically responsive bilayered  $\text{V}_2\text{O}_5$  structure with the adjustable intralayer spacing that accommodates the intercalation of  $\text{Na}^+$  ions (Figure 3C).<sup>45</sup> Because of a larger interlayer spacing ( $13.5 \text{ \AA}$  versus  $4.4 \text{ \AA}$ ), the bilayered  $\text{V}_2\text{O}_5$  electrode possessed a larger specific capacity of  $250 \text{ mAh g}^{-1}$  than orthorhombic  $\text{V}_2\text{O}_5$  ( $150 \text{ mAh g}^{-1}$ ) (Figure 3D). Moreover, the smooth slope in the charge/discharge curves indicated the solid-solution intercalation mechanism in the bilayered  $\text{V}_2\text{O}_5$ , which was different from the two-phase transitions in the orthorhombic  $\text{V}_2\text{O}_5$  electrode.

Ni/Mn-rich cathode materials have received extensive attention for advanced LIBs due to their high specific capacity.<sup>81</sup> However, these kinds of materials suffer from capacity loss and structure deterioration, which relate to a phenomenon called “cation mixing” and surface side reactions. Therefore, bulk phase and surface phase

control are developed to solve these problems, respectively. Cation-disordered lithium-excess metal oxides are a typical example of bulk phase control. Lee et al. reported a new cation-disordered material,  $\text{Li}_{1.211}\text{Mo}_{0.467}\text{Cr}_{0.3}\text{O}_2$ , in which the disordered cation mixing was induced by electrochemical cycles (Figure 3E).<sup>46</sup> Cation disorder can result in a large Li excess, which surpasses the percolation threshold and thus leads to more 0-TM channel percolating with relatively low migration barrier. This is the reason for the unexpected properties of cation-disordered materials.

Surface phase control mainly refers to the surface coating with specific material or direct surface treatment of the bulk materials, which appears to be a convenient and versatile method to improve the properties of Ni-rich materials.<sup>82,83</sup> Liu et al. have successfully synthesized a hybrid surface protection layer composed of  $\text{Mg}^{2+}$  pillar and Li-Mg-PO<sub>4</sub> layer in  $\text{Li}_{1.17}\text{Ni}_{0.17}\text{Co}_{0.17}\text{Mn}_{0.5}\text{O}_2$  (Figure 3F).<sup>47</sup> The surface protection layers can not only protect the Li insertion oxide from HF attack in electrolyte and reduce metal dissolution, but also stabilize the bulk and surface structure due to the pillar effect of the doped  $\text{Mg}^{2+}$ . Therefore, the as-synthesized material exhibits much enhanced cycling stability at 60°C, maintaining 72.6% capacity retention (180 mAh g<sup>-1</sup>) after 250 cycles. In fact, many other types of coating materials (e.g., vanadium oxide,  $\text{LiMnO}_3$ ,  $\text{AlF}_3$ ,  $\text{LiAlO}_2$ ,  $\text{LiFePO}_4$ ,  $\text{Li}_3\text{PO}_4$ , and  $\text{Li}_2\text{SO}_4$ ) have been explored for improving the charge-discharge stability of layered oxides.<sup>84–90</sup>.

#### Strain Accommodation

The large variations of ion concentration (e.g.,  $\text{Li}^+$ ,  $\text{Na}^+$ ) in insertion-type electrode materials during the charge/discharge processes will cause microstrain generation.<sup>91,92</sup> Microstrain directly leads to the structural degradation and the formation of microcracks, which cause reduced inner-particle connectivity, increased polarization, and infiltration of the electrolyte, thus leading to bad cycle stability of the materials. For example, upon delithiation of a typical  $\text{LiFePO}_4$  cathode material, a two-phase transformation occurred to form the  $\text{FePO}_4$  host.<sup>12</sup> Furthermore, the volume change associated with this phase transformation is ~6.8%.<sup>92</sup> The edge dislocations in as-cycled  $\text{LiFePO}_4$  were clearly observed via high-resolution TEM. Recently, Yan et al. used advanced scanning TEM (STEM) to investigate the nucleation and growth of intragranular cracks induced from stress in a commercial  $\text{LiNi}_{1/3}\text{Mn}_{1/3}\text{Co}_{1/3}\text{O}_2$  cathode, which led to drastic changes in crystal structures during the lithiation/delithiation process and, hence, fast capacity decay in LIBs.<sup>93</sup> Therefore, it is a great challenge to accommodate the induced strain and avoid microcracks in insertion-type electrode materials during the cycling process.

The optimization of unit cells, the increase of interface connectivity, and the design of nanostructures in electrode materials are three typical methods used to solve the aforementioned problems. Recently, Zhou et al. reported unique changes in opposite directions for  $\text{Li}_2\text{MoO}_3$  during the lithium insertion and extraction.<sup>48</sup> From *in situ* X-ray diffraction (XRD) analysis, all of the peaks shifted to low angles after delithiation (Figures 4A–4C). This phenomenon can be utilized to compensate the lattice parameter changes of electrode materials to accommodate the internal strain during the cycle process. Similarly, Wang et al. developed a new zero-strain layered material ( $\text{P2-Na}_{0.66}[\text{Li}_{0.22}\text{Ti}_{0.78}]\text{O}_2$ ), which exhibited outstanding cycling performance for SIBs.<sup>49</sup> In addition, to increase the interface connectivity and avoid the cracks of  $\text{LiNi}_{0.8}\text{Co}_{0.15}\text{Al}_{0.05}\text{O}_2$  (NCA) secondary particles, Kim et al. developed a glue-nano-filler layer (termed the G-layer) between the grains of the NCA cathode materials, which consisted of middle-temperature  $\text{Li}_x\text{CoO}_2$  ( $x < 1$ ) with a spinel-like structure

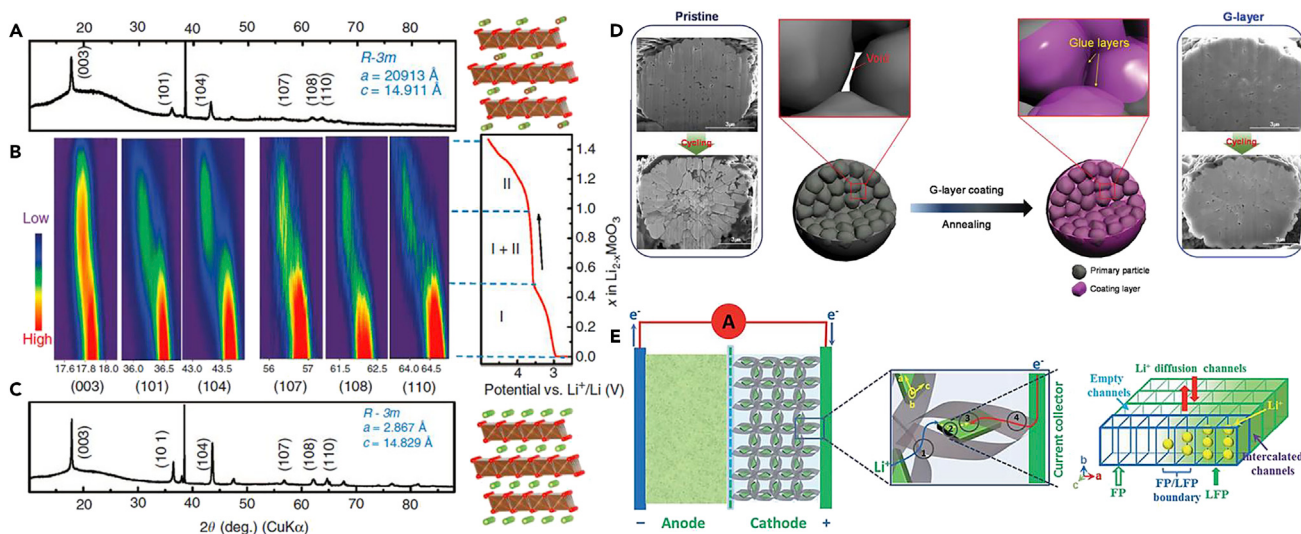


**Figure 4. Typical Examples of Battery Electrode Materials Based on Strain Accommodation**

- (A) The XRD pattern of the  $\text{Li}_{2-x}\text{MoO}_3$  after charging to 4.8 V.
- (B) *In situ* XRD pattern of the  $\text{Li}_2\text{MoO}_3$  electrode tested during the delithiation at a current density of  $10 \text{ mA g}^{-1}$  from the open-circuit voltage to 4.8 V.
- (C) The XRD pattern of the  $\text{Li}_2\text{MoO}_3$  electrode before charging. Reprinted with permission from Zhou et al.<sup>48</sup> Copyright 2014, Macmillan Publishers Limited.
- (D) The scheme shows a formation of glue layer (purple) in an NCA secondary particle (gray) during the coating processes. Cross-sectional scanning electron microscopy images of the pristine and G-layer samples before and after cycles, respectively. Reprinted with permission from Kim et al.<sup>50</sup> Copyright 2016, Wiley-VCH.
- (E) Schematic of a battery based on  $\text{LiFePO}_4$  nanoplatelets wrapped in a nitrogen-doped graphene aerogel. Reprinted with permission from Wang et al.<sup>51</sup> Copyright 2015, Royal Society of Chemistry.

(Figure 4D).<sup>50</sup> Outstanding capacity retention of 87% after 300 cycles at  $60^\circ\text{C}$  can be achieved by the introduction of the G-layer. The coating layer was able to only effectively protect the unstable surface of primary particles of the Ni-rich cathode during cycles, but also enhance the mechanical strength and electronic conductivity of a secondary particle. Finally, the design of nanostructured materials is also considered to realize the strain accommodation due to the size effect, such as  $\text{LiFePO}_4$  nanoplatelets (Figure 4E), porous  $\text{LiFePO}_4$  microspheres, and  $\text{LiNi}_{1/3}\text{Co}_{1/3}\text{Mn}_{1/3}\text{O}_2$  nanoparticles.<sup>51,94,95</sup>

#### Ion Doping

The introduction of doped ions into intrinsic crystal structures of electrode materials is a simple and efficient approach to regulate the ion diffusion channel and improve the structural stability, thereby resulting in high rate capability and long-term cycling life. Recently, Wang et al. reported a Ti-substituted  $\text{Na}_{0.44}\text{MnO}_2$  ( $\text{Na}_{0.44}[\text{Mn}_{1-x}\text{Ti}_x]\text{O}_2$ ) electrode material with a tunnel structure for aqueous SIBs.<sup>52</sup> The large S-shaped tunnel and small hexagonal tunnel in  $\text{Na}_{0.44}[\text{Mn}_{0.44}\text{Ti}_{0.56}]\text{O}_2$  were clearly revealed with Na atoms filled in (Figures 5A and 5B). The  $\text{Na}_{0.44}[\text{Mn}_{0.44}\text{Ti}_{0.56}]\text{O}_2$  electrode exhibited lower polarization, better cycling stability, and smoother charge/discharge curves, indicating an excellent structural stability and a low ion diffusion barrier (Figure 5C).

Recently, Li-/Mn-rich layered oxides have been considered as promising cathode materials for the next-generation LIBs due to their high capacity ( $\sim 300 \text{ mAh g}^{-1}$ ).<sup>81</sup> Unfortunately, several fatal drawbacks restrict their further application, such as large initial irreversible capacity and poor rate performance, as well as severe capacity and voltage fading because of the release of  $\text{O}_2$  from the crystal

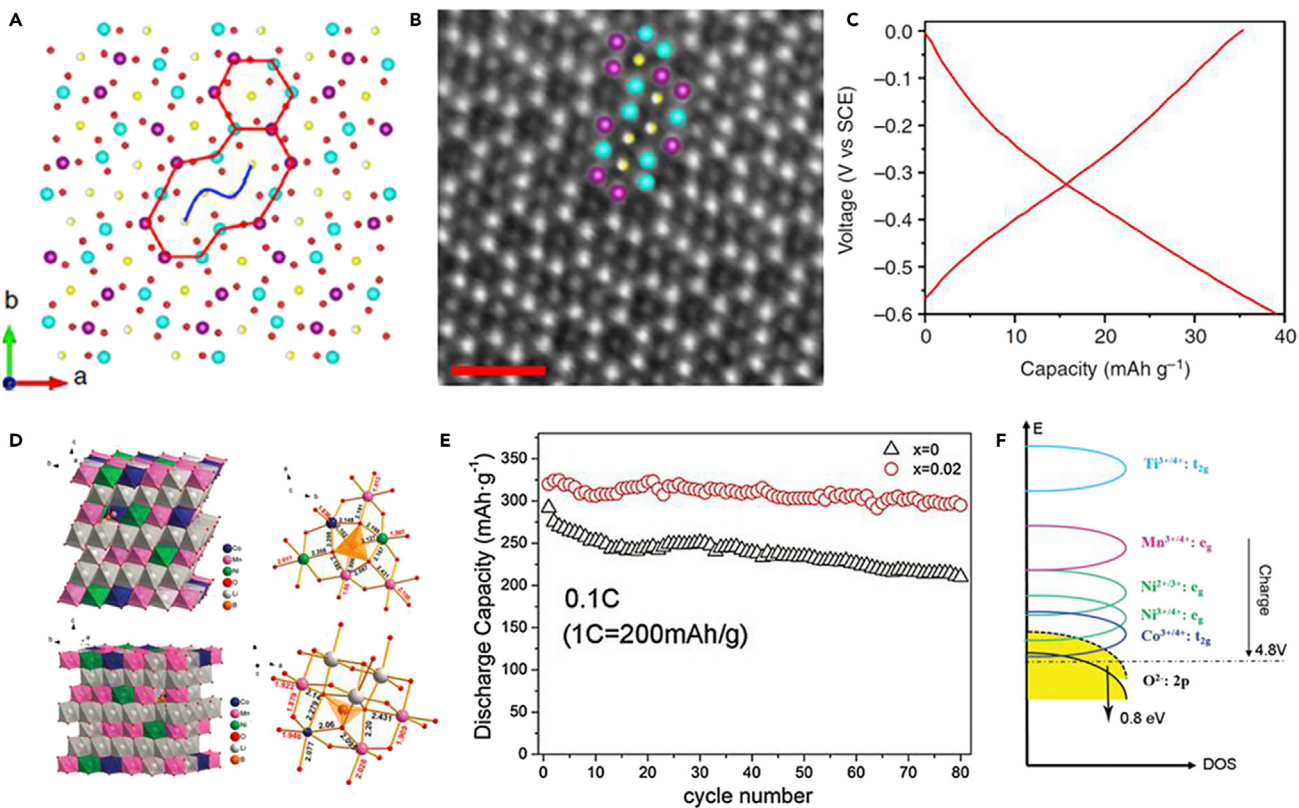


**Figure 5. Typical Examples of Battery Electrode Materials Based on Ion Doping**

- (A) Schematics of the crystal structure of  $\text{Na}_{0.44}[\text{Mn}_{0.44}\text{Ti}_{0.56}]O_2$  along [001] zone axis.
- (B) HAADF-STEM image of the as-prepared  $\text{Na}_{0.44}[\text{Mn}_{0.44}\text{Ti}_{0.56}]O_2$  material along [001] zone axis. Scale bar, 1 nm.
- (C) The first charge/discharge curves of  $\text{Na}_{0.44}[\text{Mn}_{0.44}\text{Ti}_{0.56}]O_2$  electrode in the voltage range from  $-0.6$  to  $0$  V versus SCE at a current density of  $2$  C. Reprinted with permission from Wang et al.<sup>52</sup> Copyright 2015, Macmillan Publishers Limited.
- (D) Schematic of the optimized crystal structure and bond lengths of Li-rich manganese-based oxide with  $\text{BO}_4$  and  $\text{BO}_3$  doping, respectively.
- (E) Cycling performance of undoped ( $x = 0$ ) and doped ( $x = 0.02$ ) Li-rich manganese-based oxide at  $20 \text{ mA g}^{-1}$ .
- (F) Schematic of the charge compensation mechanism before and after the boracic polyanions substitution. Reprinted with permission from Li et al.<sup>96</sup> Copyright 2014, Wiley-VCH.

lattices and the phase transformation during cycling. An ion doping strategy is considered to be able to stabilize the host materials and enhance long cycle stability.<sup>53,97</sup> Li et al. reported a strategy to improve the electrochemical performance of this host material through incorporation of boracic polyanions.<sup>96</sup> Density functional theory (DFT) results showed that the introduction of boron atoms can efficiently modulate the electronic structures of the host material due to the strong B-O bond (Figure 5D). After 80 cycles, the as-prepared doped Li-rich manganese-based oxide exhibited a higher specific capacity of  $300 \text{ mAh g}^{-1}$  and a higher capacity retention of 94% compared with undoped material ( $210 \text{ mAh g}^{-1}$  and 70%) (Figure 5E). From the Fermi energy level perspective, efficient boron doping can decrease the M-O covalency and lower the O 2p band top ( $\sim 0.8 \text{ eV}$ ) compared with those of pristine  $\text{Li}[\text{Li}_{0.2}\text{Ni}_{0.13}\text{Co}_{0.13}\text{Mn}_{0.54}]O_2$  (Figure 5F). Similarly, many doping ions have also been introduced into the crystal structure of olivine  $\text{LiFePO}_4$ , including  $\text{Mg}^{2+}$ ,  $\text{Nb}^{5+}$ ,  $\text{Cr}^{3+}$ ,  $\text{V}^{3+}$ ,  $\text{Ca}^{2+}$ , and  $\text{Zn}^{2+}$ .<sup>54–59</sup>

#### Synergistic Effect

Every type of electrode material exhibits its intrinsic characteristic features in battery performance. Therefore, the introduction of a synergistic effect between different

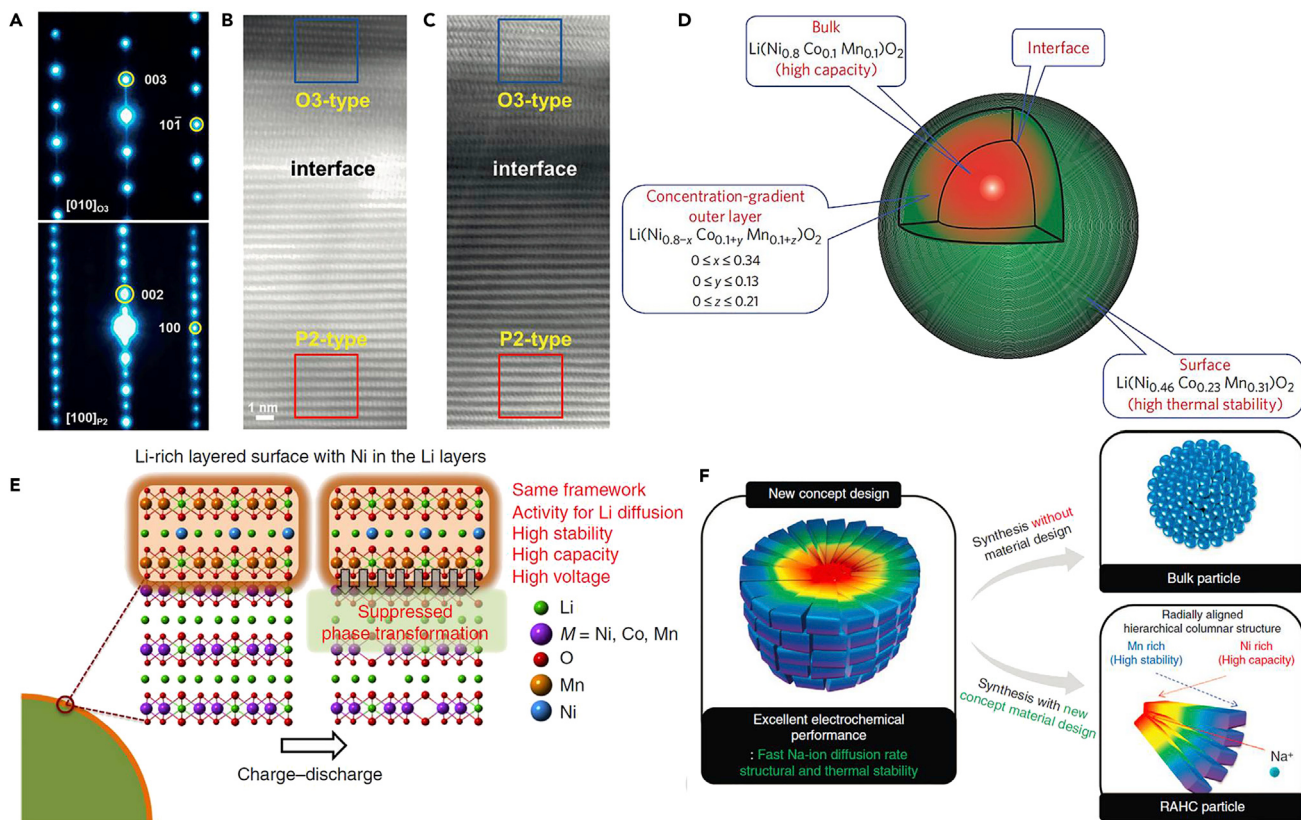


**Figure 6. Typical Examples of Battery Electrode Materials Based on Synergistic Effect**

(A) SAED patterns of O3-type structure (top) and P2-type structure (bottom) in the P2 + O3 NaLiMNC composite.

(B and C) HADDF (B) and ABF (C) images of the P2 + O3 NaLiMNC composite. Reprinted with permission from Guo et al.<sup>60</sup> Copyright 2015, Wiley-VCH. (D) Schematic of positive electrode particle with Ni-rich core surrounded by concentration-gradient outer layer. Reprinted with permission from Sun et al.<sup>61</sup> Copyright 2009, Macmillan Publishers Limited.

(E) Crystal structures near the surfaces of Li-rich layered oxides with Li-rich layered surface. Reprinted with permission from Kim et al.<sup>62</sup> Copyright 2016, Macmillan Publishers Limited.

(F) Schematic design for a RAHC particle compared with a bulk particle. Reprinted with permission from Hwang et al.<sup>63</sup> Copyright 2015, Macmillan Publishers Limited.

structures to form a new integrated electrode material provides an important way to develop high-performance batteries. According to the aforementioned discussion, sodium ions can directly migrate between two face-shared trigonal prismatic sites with a low diffusion barrier in a P2-type layered framework. However, when charging to a high voltage, the overextraction of sodium ions in the sodium layers leads to the structural degradation. In contrast, the O3 structure exhibits excellent cycling stability, but the interstitial tetrahedral sites in the O3 structure limit the sodium diffusion. To combine both advantages, Guo et al. developed a layered composite with the integration of both P2 and O3 structures ( $\text{Na}_{0.66}\text{Li}_{0.18}\text{Mn}_{0.71}\text{Ni}_{0.21}\text{Co}_{0.08}\text{O}_{2+\delta}$ , termed P2 + O3 NaLiMNC composite) to achieve outstanding performance in SIBs.<sup>60</sup> An atomic-resolution spherical aberration-corrected STEM technique was used to analyze the detailed local structure of the P2 + O3 NaLiMNC composite (Figures 6A–6C). Apparently, the superior sodium storage performance is attributed to the synergistic effect in the P2 + O3 NaLiMNC composite. Sun et al. reported a concentration-gradient cathode material with high reversible capacity and excellent cycling stability for rechargeable lithium batteries based on a layered lithium nickel cobalt manganese oxide (Figure 6D).<sup>61</sup> These

superior performances are attributed to the high capacity of the core Ni-rich composition of  $\text{Li}[\text{Ni}_{0.8}\text{Co}_{0.1}\text{Mn}_{0.1}]\text{O}_2$ , and the stability of the concentration-gradient outer layer and the surface composition of  $\text{Li}[\text{Ni}_{0.46}\text{Co}_{0.23}\text{Mn}_{0.31}]\text{O}_2$ .

Recently, to improve the cycling stability of Li-rich layered oxides without sacrificing high capacity, Kim et al. developed an Li-rich layered surface, which possessed a similar framework with the host and regularly arranged nickel between the transition metal layers (Figure 6H).<sup>62</sup> This surface structure mitigated unwanted phase transitions of the host Li-rich layered oxides, hence improving the reversible capacity and cycling stability. Besides the application in LIBs, Hwang et al. developed a radially aligned hierarchical columnar structure (RAHC) in spherical particles with various chemical compositions as an SIB cathode material (Figure 6I).<sup>63</sup> In this new design concept, the inner Ni-rich layered oxide core ( $\text{Na}[\text{Ni}_{0.75}\text{Co}_{0.02}\text{Mn}_{0.23}]\text{O}_2$ ) exhibited a high capacity due to more Ni-based redox reactions involved; meanwhile, the outer Mn-rich layered oxide shell ( $\text{Na}[\text{Ni}_{0.58}\text{Co}_{0.06}\text{Mn}_{0.36}]\text{O}_2$ ) displayed high stability. In addition, a variety of other functional electrode materials with synergistic structures have been developed for high-performance batteries.<sup>64,98–101</sup>

### Optimization Strategies for Alloying-/Conversion-type Materials

Alloying-/conversion-type materials have been intensively studied as promising anode candidates for new-generation batteries due to their abundant sources, easy preparation, low cost, and high theoretical capacities. On the basis of design principles, the intrinsic high theoretical capacities are attributed to their excellent host chemistry that stores more energy. However, the concomitant large volume variation, low conductivity, voltage hysteresis, and instability of the SEI film are major problems for further practical applications in batteries. In this section, we try to elucidate the structure-property relationship mainly from the phase structure perspective. Phase-buffering strategy includes the introduction of inert component phases and the crystallinity degree control, aiming to alleviate the volume expansion and improve the cycle stability; the continuous conductive phase strategy includes the construction of internal and external conductive networks and the control of SEI, with the purpose of solving the problem of slow electron and ion transport and voltage hysteresis; the synergistic effect highlights the novel conversion/alloying materials, where the metallic particles during the cycling process play a critical role in improving the overall performance (Table 1).

#### Phase-Buffering Mechanism

To accommodate the large volume variation during the ion insertion/extraction process, the introduction of a phase-buffering mechanism in the electrode materials is of great significance in improving cycling stability for batteries. One method is to introduce inactive ingredients into the active conversion-/alloying-type electrode materials. For example, the schematic of the reversible Li insertion/extraction process in  $\text{CaFe}_2\text{O}_4$  is shown in Figure 7A.<sup>65</sup> Due to a strong metal-oxygen bond, the *in situ* generated  $\text{CaO}$  nanograins in electrode materials was inactive, which can efficiently buffer the large volume variation and suppress the agglomeration of active  $\text{Fe}_2\text{O}_3$  during the cycling process, resulting in excellent cycling stability. Kim et al. developed a new active/inactive layered electrode material, namely  $\text{Ca}_3\text{Co}_4\text{O}_9$ , which exhibited enhanced cycling performance and rate capability in LIBs.<sup>66</sup> In addition, intermetallic compounds, termed MM' composition (where M' does not alloy with lithium), have also received much attention. The inactive M' can essentially alleviate the volume expansion and improve the conductivity of electrode materials, thereby improving the cycling stability of alloying materials.<sup>67</sup> Recently, Liu et al. reported an intermetallic compound,  $\text{Ni}_3\text{Sn}_2$ , as the anode materials in LIBs and

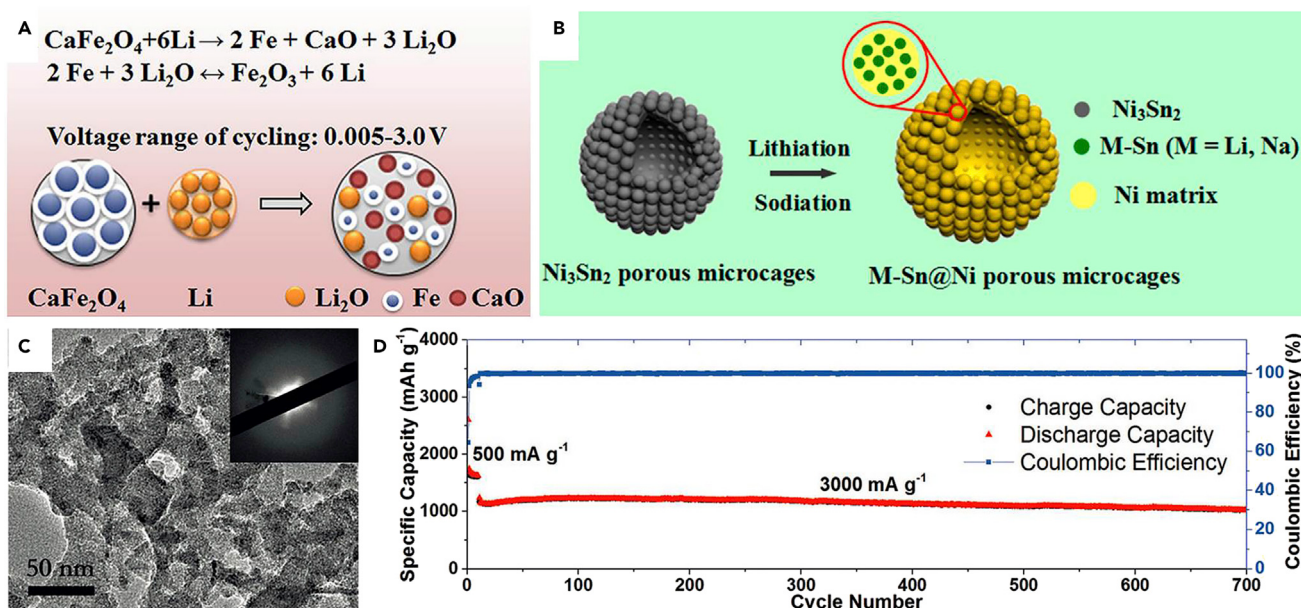


**Figure 7. Typical Examples of Battery Electrode Materials Based on Phase-Buffering Mechanism**

(A) Schematic of reversible Li insertion and extraction process of CaFe<sub>2</sub>O<sub>4</sub>. Reprinted with permission from Reddy et al.<sup>65</sup> Copyright 2013, American Chemical Society.

(B) Schematic of the first lithiation and sodiation of porous Ni<sub>3</sub>Sn<sub>2</sub> intermetallic microcages. Reprinted with permission from Liu et al.<sup>68</sup> Copyright 2014, American Chemical Society.

(C) TEM image of mesoporous amorphous silicon; inset shows SAED pattern.

(D) Cycling performance and coulombic efficiency of porous amorphous Si at a current density of 3,000 mA g<sup>-1</sup>. Reprinted with permission from Liu et al.<sup>69</sup> Copyright 2016, Wiley-VCH.

SIBs.<sup>68</sup> After the first lithiation and sodiation, porous Ni<sub>3</sub>Sn<sub>2</sub> intermetallic microcages were transformed into M-Sn@Ni (M = Li, Na) porous microcages with the electroactive M-Sn particles embedded in a 3D conducting Ni hollow matrix (Figure 7B). The presence of the inactive Ni matrix contributes to the superior electrochemical performances of Ni<sub>3</sub>Sn<sub>2</sub> in LIBs and SIBs. In brief, all these results demonstrated that the introduction of inactive ingredients with buffering mechanisms into the active-component containing electrodes is an efficient approach to improve the electrochemical performances in batteries. However, on the other hand the inactive ingredients can also reduce the specific capacity of the whole electrode materials.

Another efficient approach used to avoid sacrificing the capacity due to the addition of inactive ingredients is to reduce the crystalline degree of alloying-type and conversion-type materials. For instance, compared with crystalline Si, the isotropic strain and rich inner voids in amorphous Si can accommodate the large volume variation and restrain the particle pulverization. Recently Lin et al. synthesized amorphous Si, which exhibited excellent electrochemical performance in LIBs with a high reversible capacity of 1,025 mAh g<sup>-1</sup> and 93% capacity retention after 700 cycles at 3 A g<sup>-1</sup> (Figures 7C and 7D).<sup>69</sup>

#### Continuous Conductive Phase Control

The control of the continuous conductive phase in conversion-/alloying-type materials is important in realizing high reversible capacity and good cycling stability. For some reversible conversion-type materials such as metal oxides (e.g., Fe<sub>2</sub>O<sub>3</sub>, Co<sub>3</sub>O<sub>4</sub>) and fluorides (e.g., CoF<sub>2</sub>, FeF<sub>2</sub>, FeF<sub>3</sub>), their good cycling characteristics can be attributed to the *in situ* formation of fine and continuous metallic nanoparticles

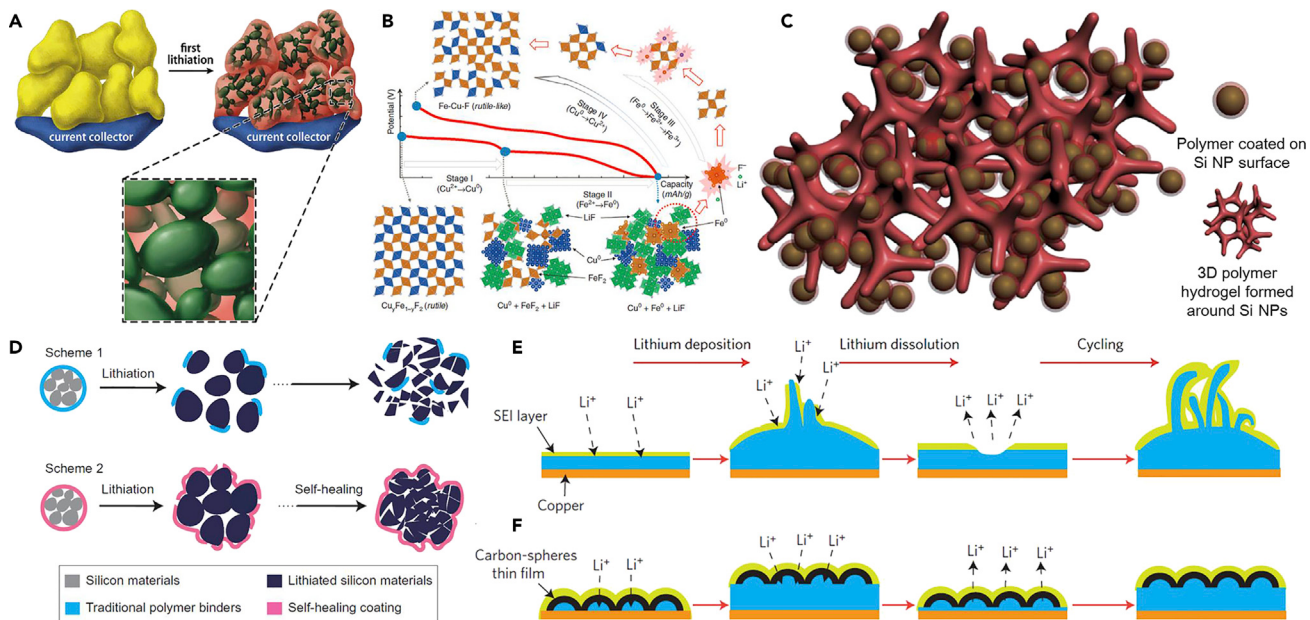


**Figure 8. Typical Examples of Battery Electrode Materials Based on Continuous Conductive Phase Control**

(A) Schematic for the conversion of the  $\text{FeF}_2$  agglomerates into a bicontinuous network of  $\text{Fe}$  nanoparticles and  $\text{LiF}$  during the first lithiation process. Reprinted with permission from Wang et al.<sup>102</sup> Copyright 2011, American Chemical Society.

(B) Schematic of the asymmetric reaction pathway in  $\text{Cu}_y\text{Fe}_{1-y}\text{F}_2$ . Reprinted with permission from Wang et al.<sup>71</sup> Copyright 2015, Macmillan Publishers Limited.

(C) Schematic of 3D porous SiNP/conductive polymer hydrogel composite electrodes. Reprinted with permission from Wu et al.<sup>72</sup> Copyright 2013, Macmillan Publishers Limited.

(D) Schematics of the design and behavior of a conventional silicon electrode (Scheme 1) and a stretchable self-healing electrode (Scheme 2). Reprinted with permission from Wang et al.<sup>19</sup> Copyright 2013, Macmillan Publishers Limited.

(E and F) Schematics of the different Li anode structural evolution during cycling with pure Cu (E) and modified Cu (F) with a hollow carbon nanosphere layer as the substrates, respectively. Reprinted with permission from Zheng et al.<sup>77</sup> Copyright 2014, Macmillan Publishers Limited.

embedded in an insulating matrix ( $\text{Li}_2\text{O}$  or  $\text{LiF}$ ) (Figure 8A).<sup>70,102</sup> It is noted that  $\text{FeF}_3$  as a cathode material exhibits higher theoretical capacity ( $712 \text{ mAh g}^{-1}$ ), higher thermodynamic reduction potential (2.74 V), and weaker reaction reversibility than those of  $\text{FeF}_2$  ( $571 \text{ mAh g}^{-1}$ , 2.66 V). However, without a continuous conductive network, the electrochemical processes in some conversion-type materials, such as  $\text{CuF}_2$ , are irreversible. To realize the reversibility of Cu-based fluoride electrode, Wang et al. fabricated ternary metal fluorides ( $\text{Cu}_y\text{Fe}_{1-y}\text{F}_2$ ), which exhibited reversible Cu and Fe redox reactions with small hysteresis (<150 mV) (Figure 8B).<sup>71</sup> The reversibility of Cu-based ternary fluorides is attributed to the formation of continuous metallic phases during the conversion reaction process.

It is noteworthy that the formation of continuous conductive phase in alloying-type materials is mainly blocked by SEI films because their Fermi energy levels are lower than the LUMO of organic electrolyte. Wu et al. designed and constructed high-performance Li-ion battery negative electrodes by encapsulating Si nanoparticles (SiNPs) in a nanostructured 3D porous conductive polymer framework (Figure 8C).<sup>72</sup> The proposed nanodomain-confined crystallization in a conductive polymer matrix enabled a continuous reversible crystalline-phase transformation and so controlled the formation of a stable SEI on the SiNP surface. The 3D nanostructured gel network also promotes electron transport along the backbone, facilitates the diffusion of ions through hierarchical pores, and provides a high surface area for interfacial reactions, which can generally extend their energy-related applications.<sup>73–75</sup> Meanwhile,

Wang et al. applied self-healing chemistry to silicon microparticles to maintain electrical contact between the broken particles, to realize no cracks in the polymer binder and the formation of stable SEI during cycling (Figure 8D).<sup>19</sup> Similarly, other smart architectures endow active silicon particles with enhanced electrochemical performances.<sup>18,76,103</sup>

In addition, lithium metal is another promising battery anode due to its highest theoretical capacity (3,860 mAh g<sup>-1</sup>) and lowest electrochemical potential among all possible candidates (e.g., commercial graphite and Li<sub>4</sub>Ti<sub>5</sub>O<sub>12</sub>).<sup>104</sup> However, previous investigations have revealed that inhomogeneous mass and charge transfers across the Li/electrolyte interface lead to the formation of dendritic Li and “dead” Li along with large volume change, and an unstable SEI upon repeated plating/stripping cycles, which seriously limited its applications in rechargeable batteries (Figure 8E).<sup>77</sup> Recently, Zheng et al. demonstrated that coating the lithium metal anode with a monolayer film of interconnected amorphous hollow carbon nanospheres efficiently controlled the lithium metal depositions under the carbon film (Figure 8F).<sup>77</sup> This smart architecture on nanoscale interfacial engineering facilitated the formation of a stable SEI and a continuous conductive phase of Li metal, which exhibited improved electrochemical performance. To realize the continuous conductive phase of Li metal, many other strategies have been developed for stabilizing the SEI of lithium metal anodes, such as electrolyte engineering and lithium overcoating.<sup>105,106</sup>

#### Synergistic Effect

Pure alloying-type or conversion-type materials suffer from various problems such as low coulombic efficiency, volume expansion, and large voltage hysteresis. By combining both advantages, new-type conversion/alloying materials have been developed, for example, ZnTM<sub>2</sub>O<sub>4</sub> (with TM = Fe, Co, Mn).<sup>78</sup> In these conversion/alloying materials, a very fine distribution of the alloying element at the atomic scale can accommodate large volume expansion during the cycling process, improve the conductivity, and facilitate the particle morphology evolution of conversion-type materials; on the other hand, the formed Li<sub>2</sub>O and TM nanonetworks from conversion-type materials can also buffer the alloying reaction. This synergistic effect endows these conversion/alloying materials with enhanced electrochemical performance (Figure 9A).<sup>78</sup>

The synergistic effect among multiphase components was also introduced into conversion-/alloying-type materials to build multiple interacting interfaces for high-performance batteries. Jiang et al. developed a high fraction of highly interconnected interfaces of Fe/Sn/Li<sub>2</sub>O in SnO<sub>2</sub>-Fe<sub>2</sub>O<sub>3</sub>-Li<sub>2</sub>O nanocomposites during the initial cycles (Figure 9B).<sup>79</sup> The generated Fe metal and the pre-introduced Li<sub>2</sub>O can provide fast channels for the transfer of electrons and Li<sup>+</sup> ions, respectively. After the conversion reaction of SnO<sub>2</sub>, the formed ultra-small Sn nanodots exhibited abundant active sites, high pseudo-capacitive storage, and fast reaction kinetics. The synergistic effect in highly interconnected interfaces enabled fast electrochemical reactions, structural integrity and long-term stability for LIBs. The Sn-based nanocomposite delivered a high reversible capacity of 420 mAh g<sup>-1</sup>, an excellent rate capability, and a high-capacity retention of 80% after 1,200 cycles at 1 A g<sup>-1</sup>. On the other hand, the introduction of transition metals in alloying metal oxides such as ZnO or SnO<sub>2</sub> is another efficient approach. Hu et al. reported a series of ternary SnO<sub>2</sub>-M-graphite composites (M = Fe, Mn, Co) by a simple ball-milling method (Figure 9C).<sup>80</sup> The catalytic effect of M played an important role in accelerating the conversion of Sn/Li<sub>2</sub>O to SnO<sub>2</sub>; meanwhile, the nanosized M could act as the

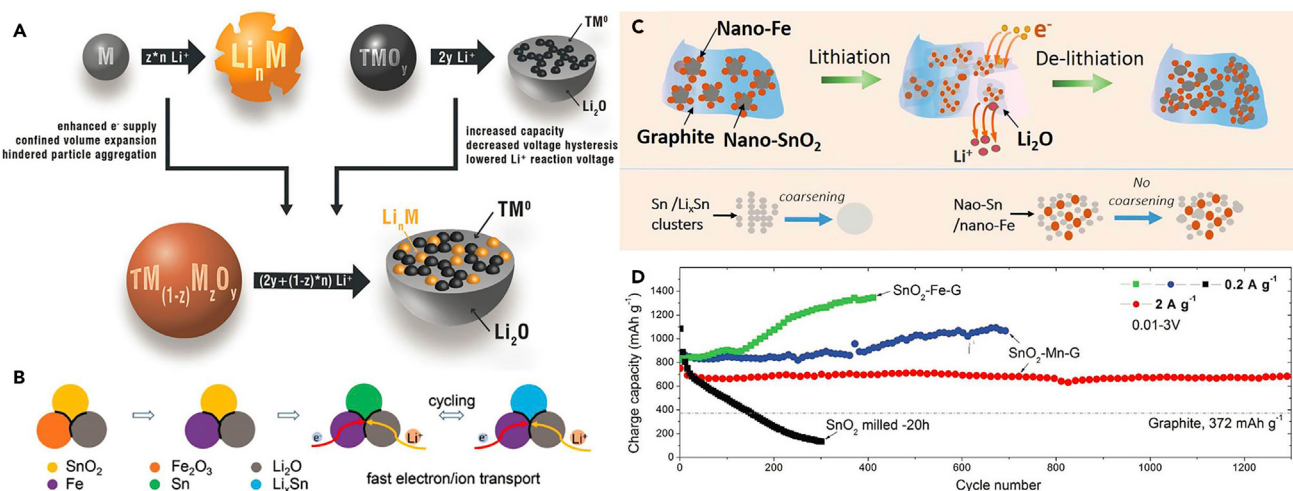


**Figure 9. Typical Examples of Battery Electrode Materials Based on Synergistic Effect**

(A) Schematic of the advantages by combining conversion-type and alloying-type Li storage in conversion/alloying materials. Reprinted with permission from Bresser et al.<sup>78</sup> Copyright 2016, Royal Society of Chemistry.

(B) Schematic of intimate and well-distributed contacts among the Fe, Sn, and  $\text{Li}_2\text{O}$  nanoparticles, realizing fast electron/Li<sup>+</sup> transport. Reprinted with permission from Jiang et al.<sup>79</sup> Copyright 2017, Wiley-VCH.

(C) Schematics for the high reversibility reactions in ternary  $\text{SnO}_2\text{-M}$ -graphite nanocomposites.

(D) Cycling performance of the  $\text{SnO}_2\text{-Fe-G}$  nanocomposite,  $\text{SnO}_2\text{-Mn-G}$  nanocomposite, and  $\text{SnO}_2$  milled-20 hr at 0.2 A g<sup>-1</sup>. Reprinted with permission from Hu et al.<sup>80</sup> Copyright 2017, Wiley-VCH.

barriers to suppress the aggregation and long-distance diffusion of Sn owing to the formation of the interfacial intermetallic  $\text{Sn}_x\text{M}_y$  phase. On the basis of the synergistic effect, the  $\text{SnO}_2\text{-Fe}$ -graphite and  $\text{SnO}_2\text{-Mn}$ -graphite electrodes exhibited a high reversible capacity of 1,338 mAh g<sup>-1</sup> after 400 cycles at 0.2 A g<sup>-1</sup>, and a long-term stable capacity of 700 mAh g<sup>-1</sup> after 1,300 cycles at 2 A g<sup>-1</sup>, respectively (Figure 9D).

### Advanced Techniques on Battery Electrode Materials

According to aforementioned discussions on the understanding and optimization strategies of electrode materials, the in-depth fundamental study and the further discovery of optimization strategies are critical in making major breakthroughs for next-generation rechargeable batteries. This part focuses on the advanced techniques used to study electrode materials, including micro-/nanoscale electrochemical devices for direct probing, high-resolution structure characterizations, and theoretical calculations.

#### Micro/Nanoscale Electrochemical Devices for Direct Probing

The in-depth investigations of electrode materials are of great influence in achieving high performance for energy storage devices. In real energy storage devices the active electrode materials are mixed with the electrolytes, binders, and conductive additives, which greatly hinder the exploration of electrochemical processes in traditional testing. Therefore, micro-/nanoscale electrochemical devices have been developed and exploited to be a powerful diagnostic tool, which can provide direct probing of the electrochemical properties by using a single nanostructure at the nanoscale scope. To understand the electrode capacity fading in energy storage devices, Mai et al. designed and assembled the smallest all-solid single-nanowire electrochemical devices for *in situ* probing, consisting of a single Si nanowire as the working electrode, the  $\text{LiCoO}_2$  nanofilm as the counter electrode, and the

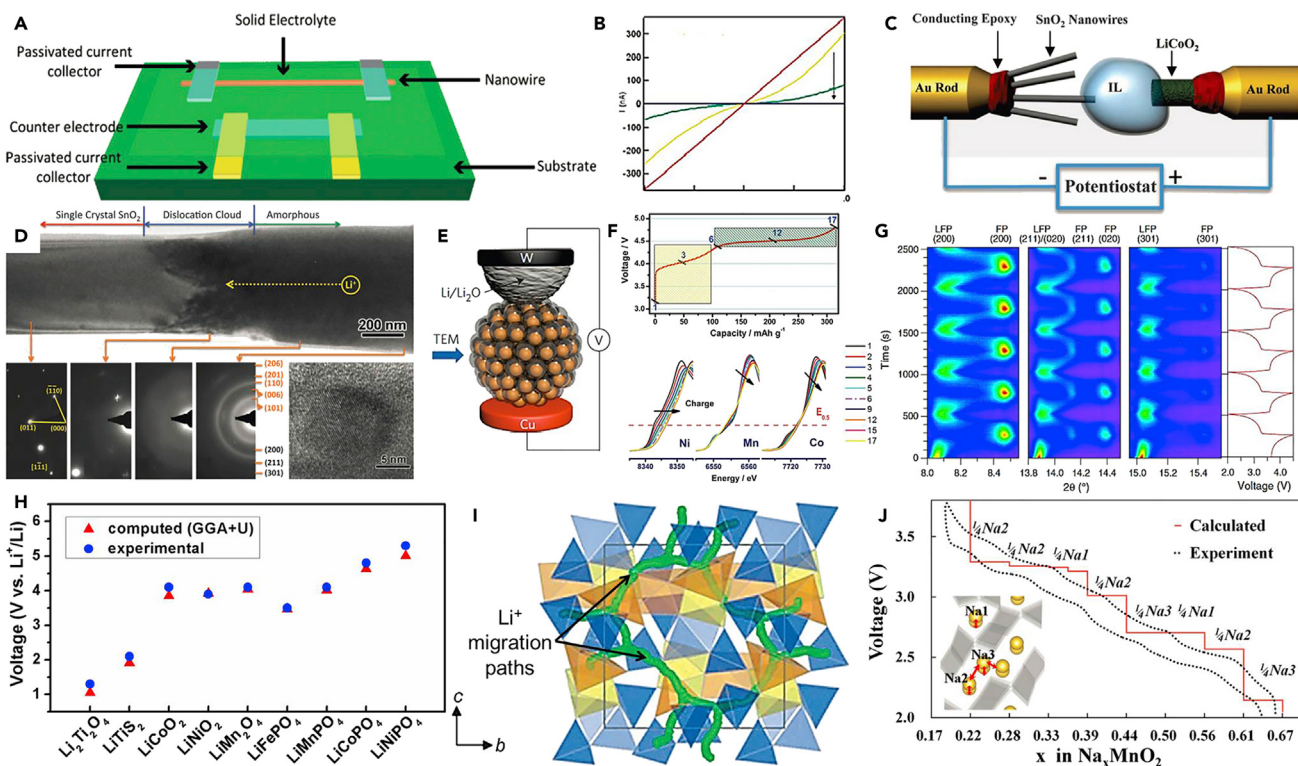


**Figure 10. Typical Examples of Advanced Techniques on Battery Electrode Materials**

- (A) Schematic of a design on a single-nanowire electrode device.
- (B) Transport property evolution of Si/a-Si nanowire along with the electrochemical test. Reprinted with permission from Mai et al.<sup>107</sup> Copyright 2010, American Chemical Society.
- (C) Schematic of the TEM experimental setup based on single SnO<sub>2</sub> nanowire.
- (D) Structural and phase characterization of another SnO<sub>2</sub> nanowire anode during charging at -3.5 V against the LiCoO<sub>2</sub> cathode. Reprinted with permission from Huang et al.<sup>108</sup> Copyright 2010, American Association for the Advancement of Science.
- (E) Schematic of the *in situ* TEM device based on single Si pomegranates. Reprinted with permission from Liu et al.<sup>17</sup> Copyright 2014, Macmillan Publishers Limited.
- (F) *In situ* XAS spectra of the Li-rich layered Li<sub>1.2</sub>Ni<sub>0.15</sub>Co<sub>0.1</sub>Mn<sub>0.55</sub>O<sub>2</sub> material during the initial charge process. Reprinted with permission from Yu et al.<sup>109</sup> Copyright 2012, Wiley-VCH.
- (G) *In situ* XRD patterns during the galvanostatic charge/discharge at a rate of 10 C. Reprinted with permission from Liu et al.<sup>110</sup> Copyright 2014, American Association for the Advancement of Science.
- (H) Comparison between experimental and computed voltages. Reprinted with permission from Chevrier et al.<sup>111</sup> Copyright 2010, The American Physical Society.
- (I) Calculated paths for long-range Li<sup>+</sup> migration in Li<sub>2</sub>FeP<sub>2</sub>O<sub>7</sub> along the b-axis and c-axis directions. Reprinted with permission from Clark et al.<sup>112</sup> Copyright 2012, Wiley-VCH.
- (J) Comparison of calculated voltage profile and experimental charge/discharge curves. Reprinted with permission from Kim et al.<sup>113</sup> Copyright 2012, American Chemical Society.

PEO-LiClO<sub>4</sub>-PC-EC polymer as the electrolyte (Figure 10A).<sup>107</sup> After the initial charge/discharge cycle, the conductance of the Si nanowire irreversibly decreased by over 2 orders of magnitude, which was the key point to limit the electrochemical properties of the devices (Figure 10B).

#### High-Resolution Structure Characterization

High-resolution structure characterizations play important roles in the development and understanding of the electrode materials for energy storage devices. In previous years, many advanced characterization techniques have been developed, such as XRD, TEM, scanning electron microscopy, and X-ray photoelectron spectroscopy. Recently the spherical aberration-corrected STEM technique has become a powerful

tool for providing comprehensive information on the crystal structures of electrode materials at the atomic scale. For example, Sun et al. observed clear interfacial structures and a three-phase coexisting region at the atomic scale in sodiated  $\text{Li}_4\text{Ti}_5\text{O}_{12}$  nanoparticles.<sup>114</sup>

As the electrochemical reactions in electrode materials are dynamic, numerous *in situ* characterization methods have been developed to investigate the structural evolution of electrode materials during the dynamic electrochemical processes.<sup>115,116</sup> Huang et al. constructed a nanoscale electrochemical device inside a high-resolution TEM to observe *in situ* the electrochemical lithiation of a single  $\text{SnO}_2$  nanowire electrode (Figure 10C).<sup>108</sup> During charging, the structural and phase evolution of the nanowire were clearly revealed (Figure 10D). Cui et al. performed an *in situ* TEM study of silicon pomegranates with varied internal void spaces in lithiation (Figure 10E).<sup>17</sup> In addition, some other operando experiments, such as operando X-ray absorption spectroscopy (XAS) and operando XRD, have been used as powerful methods to understand the detailed reaction mechanisms during the charge/discharging process in batteries. Xu et al. used *in situ* XAS to elucidate the changes in the electronic transitions and local structure of the Li-rich layered  $\text{Li}_{1.2}\text{Ni}_{0.15}\text{Co}_{0.1}\text{Mn}_{0.55}\text{O}_2$  material (Figure 10F).<sup>109</sup> These results revealed that the voltage slope region (3–4.4 V) is mostly related to the oxidation of Ni and Co sites, while the voltage plateau region mostly corresponds to the Mn sites during initial charging. Using time-resolved *in situ* XRD, Liu et al. revealed the existence of a continuous metastable solid-solution phase in  $\text{LiFePO}_4$  during rapid lithium extraction and insertion (Figure 10G).<sup>110</sup>

With the development of high-resolution structure characterizations, some general phenomena and new energy storage mechanisms can be efficiently investigated, which are beneficial for understanding the intrinsic structure-property relationships. These studies will thus be helpful for the rational design of electrode materials for high-performance batteries.

#### Theoretical Calculations

Theoretical calculations are also very important in characterizing and predicting the structures and properties of complex electrode materials at the atomic scale.<sup>117</sup> In Figure 10H, lithium intercalation potentials obtained with generalized gradient approximation (GGA) + U are similar to the experimental results.<sup>111</sup> Clark et al. used simulation techniques to provide insights into the  $\text{Li}^+$  migration pathways in  $\text{Li}_2\text{FeP}_2\text{O}_7$  cathode material (Figure 10I).<sup>112</sup> Lithium diffusion in  $\text{Li}_2\text{FeP}_2\text{O}_7$  exhibited nonlinear and curved paths parallel to the b and c axes with a low migration energy (0.40 eV). Moreover, Kim et al. used DFT calculations to investigate the sodium insertion/extraction mechanisms of  $\text{Na}_{0.44}\text{MnO}_2$  (Figure 10J).<sup>113</sup> The theoretical calculation results revealed the existence of seven intermediate phases and two-phase reactions among them, whereby the corresponding calculated voltage profiles were in agreement with experimental results.

#### Conclusions and Outlook

In the past decades enormous progress has been made in battery research to achieve better understanding of the underlying structure-property relationships in electrode materials. From the perspective of battery chemistry, this review provides in-depth discussions of the battery reaction mechanisms and highlights the structure and property optimizations of battery materials for high-efficiency energy storage. In particular, three major design principles for electrode materials are summarized: (1) excellent host chemistry; (2) efficient ion and electron transport; and (3) long-term

structural stability. Furthermore, some important structure optimization strategies for insertion-, alloying-, and conversion-type electrode materials are summarized in detail.

The increase of energy demands for potential portable electronics, electric vehicles, and smart power grids requires the batteries to have improved safety, higher energy/power density, longer cycling life, and lower cost. However, many challenges still exist in making major breakthroughs in high-performance batteries for large-scale applications. To address these challenges, some important aspects on the development of battery research need to be considered.

(1) It is highly desirable to develop new electrode materials and advanced storage devices to meet the urgent demands of high energy and power densities for large-scale applications. In a real full battery, electrode materials with higher capacities and a larger potential difference between the anode and cathode materials are needed. For positive electrode materials, in the past decades a series of new cathode materials (such as  $\text{LiNi}_{0.6}\text{Co}_{0.2}\text{Mn}_{0.2}\text{O}_2$  and Li-/Mn-rich layered oxide) have been developed, which can provide a capacity of up to  $200 \text{ mAh g}^{-1}$  to replace the commercial  $\text{LiCoO}_2$  ( $\sim 140 \text{ mAh g}^{-1}$ ). In addition, as an alternative to conventional inorganic intercalation electrode materials, organic electrode materials (e.g., conductive polymers, organic carbonyl compounds, quinone/diimides/phenoxide and their derivatives) are promising candidates for the next generation of sustainable and versatile energy storage devices.<sup>118</sup> On the basis of new storage mechanisms, some new storage devices have attracted intensive interests due to their high reversible capacities and low cost, such as Li-S, magnesium-ion, zinc-ion, and metal-air batteries. However, these promising materials still suffer from some scientific problems and challenges that limit their further applications. For negative materials, lithium metal is the ultimate choice for the anode in an Li battery because of its highest theoretical capacity and lowest electrochemical potential. Apart from nanoscale interfacial engineering and liquid electrolyte engineering, developing advanced solid-state batteries is also important to effectively block Li dendrites and provide a large electrochemical stability window (0–5 V) and superior thermal stability. Solid electrolytes mainly include inorganic ceramic electrolytes (e.g.,  $\text{Li}_{10}\text{GeP}_2\text{S}_{12}$ , garnet-type  $\text{Li}_7\text{La}_3\text{Zr}_2\text{O}_{12}$ ) and solid polymer electrolytes.<sup>104</sup> However, it remains a formidable challenge to realize the comprehensive combination of high modulus to stop Li dendrite penetration, as well as obtain high Li-ion conductivity, low interfacial resistance, and good adhesion with both electrodes in one solid electrolyte.

(2) In-depth understanding of the fundamental reaction mechanisms and the structure-property correlations is urgently needed. Batteries are electrochemical devices that store energy via chemical reactions. However, detailed information about the intrinsic electrochemical reaction mechanisms in electrode materials is still limited due to their complexity and the negative effects from binders and conductive carbon additives. In this regard, the understanding of structure-property correlations also plays an important role in showing the way toward efficient optimization strategies. Meanwhile, the recently developed advanced high-resolution *in situ* characterization techniques and theoretical calculations have become powerful tools for further investigation and prediction.

(3) Low cost and practicability are crucial for large-scale applications in industry. The cost of electrode materials derives from both raw materials and fabrication processes. To replace high-cost commercial  $\text{LiCoO}_2$ , a series of earth-abundant

cathode materials have been developed, such as  $\text{LiNi}_{0.6}\text{Co}_{0.2}\text{Mn}_{0.2}\text{O}_2$  and  $\text{LiFePO}_4$ . Moreover, low-cost fabrication processes for electrode materials are important for practical applications in industry. The design of delicate nanostructured electrode materials, which show enhanced electrochemical performance in the laboratory, usually leads to complex fabrication process, low packing density, and high cost. For widespread commercial applications, however, simple, environmentally friendly, and scalable synthetic strategies are highly desired.

The development of sustainable energy relies on the comprehensive contributions from many important aspects including fundamental research, large-scale application, and market demand, as well as government policy and support. Among these factors, bridging the fundamental research in the laboratory and the scalable development in industry is extremely important. On the basis of in-depth understanding of battery chemistry in electrode materials, some important reaction mechanisms and design principles are clearly revealed herein and the strategies for structure and property optimizations summarized. This review will provide an appropriate pathway toward the rational design of ideal battery materials for large-scale applications in industry.

## AUTHOR CONTRIBUTIONS

J.M. and H.G. conducted the literature search and wrote the manuscript. J.M., C.N., Q.L., Y.Z., and L.X. discussed and revised the manuscript. L.M. proposed the topic and reviewed the manuscript. J.M. and H.G. contributed equally to this work.

## ACKNOWLEDGMENTS

This work was supported by the National Key Research and Development Program of China (2016YFA0202603), the National Basic Research Program of China (2013CB934103), the Program of Introducing Talents of Discipline to Universities (B17034), the National Natural Science Foundation of China (51521001), the National Natural Science Fund for Distinguished Young Scholars (51425204), and the Fundamental Research Funds for the Central Universities (WUT: 2016III001 and 2016-YB-004). L.M. gratefully acknowledges financial support from China Scholarship Council (No. 201606955096).

## REFERENCES

1. Stamenkovic, V.R., Strmcnik, D., Lopes, P.P., and Markovic, N.M. (2016). Energy and fuels from electrochemical interfaces. *Nat. Mater.* 16, 57–69.
2. Yang, Z., Zhang, J., Kintner-Meyer, M.C., Lu, X., Choi, D., Lemmon, J.P., and Liu, J. (2011). Electrochemical energy storage for green grid. *Chem. Rev.* 111, 3577–3613.
3. Mai, L., Tian, X., Xu, X., Chang, L., and Xu, L. (2014). Nanowire electrodes for electrochemical energy storage devices. *Chem. Rev.* 114, 11828–11862.
4. Choi, J.W., and Aurbach, D. (2016). Promise and reality of post-lithium-ion batteries with high energy densities. *Nat. Rev. Mater.* 1, 16013.
5. Patil, A., Patil, V., Shin, D.W., Choi, J.-W., Paik, D.-S., and Yoon, S.-J. (2008). Issue and challenges facing rechargeable thin film lithium batteries. *Mater. Res. Bull.* 43, 1913–1942.
6. Tang, Y., Zhang, Y., Li, W., Ma, B., and Chen, X. (2015). Rational material design for ultrafast rechargeable lithium-ion batteries. *Chem. Soc. Rev.* 44, 5926–5940.
7. Yabuuchi, N., Kubota, K., Dahbi, M., and Komaba, S. (2014). Research development on sodium-ion batteries. *Chem. Rev.* 114, 11636–11682.
8. Lu, J., Chen, Z., Ma, Z., Pan, F., Curtiss, L.A., and Amine, K. (2016). The role of nanotechnology in the development of battery materials for electric vehicles. *Nat. Nanotechnol.* 11, 1031–1038.
9. Wang, K.-X., Li, X.-H., and Chen, J.-S. (2015). Surface and interface engineering of electrode materials for lithium-ion batteries. *Adv. Mater.* 27, 527–545.
10. Peng, L., Zhu, Y., Chen, D., Ruoff, R.S., and Yu, G. (2016). Two-dimensional materials for beyond-lithium-ion batteries. *Adv. Energy Mater.* 6, 1600025.
11. Wang, L., He, X., Sun, W., Wang, J., Li, Y., and Fan, S. (2012). Crystal orientation tuning of  $\text{LiFePO}_4$  nanoplates for high rate lithium battery cathode materials. *Nano Lett.* 12, 5632–5636.
12. Paolella, A., Bertoni, G., Marras, S., Dileva, E., Colombo, M., Prato, M., Riedinger, A., Povia, M., Ansaldi, A., Zaghib, K., et al. (2014). Etched colloidal  $\text{LiFePO}_4$  nanoplatelets toward high-rate capable Li-ion battery electrodes. *Nano Lett.* 14, 6828–6835.
13. Zhao, Y., Peng, L., Liu, B., and Yu, G. (2014). Single-crystalline  $\text{LiFePO}_4$  nanosheets for high-rate Li-ion batteries. *Nano Lett.* 14, 2849–2853.
14. Dominko, R., Bele, M., Gaberscek, M., Remskar, M., Hanzel, D., Pejovnik, S., and Jamnik, J. (2005). Impact of the carbon coating thickness on the electrochemical performance of  $\text{LiFePO}_4/\text{C}$  composites. *J. Electrochem. Soc.* 152, A607–A610.

15. Meng, J., Niu, C., Xu, L., Li, J., Liu, X., Wang, X., Wu, Y., Xu, X., Chen, W., Li, Q., et al. (2017). General oriented formation of carbon nanotubes from metal-organic frameworks. *J. Am. Chem. Soc.* 139, 8212–8221.
16. Chan, C.K., Peng, H., Liu, G., McIlwrath, K., Zhang, X.F., Huggins, R.A., and Cui, Y. (2008). High-performance lithium battery anodes using silicon nanowires. *Nat. Nanotechnol.* 3, 31–35.
17. Liu, N., Lu, Z., Zhao, J., McDowell, M.T., Lee, H.-W., Zhao, W., and Cui, Y. (2014). A pomegranate-inspired nanoscale design for large-volume-change lithium battery anodes. *Nat. Nanotechnol.* 9, 187–192.
18. Ko, M., Chae, S., Ma, J., Kim, N., Lee, H.-W., Cui, Y., and Cho, J. (2016). Scalable synthesis of silicon-nanolayer-embedded graphite for high-energy lithium-ion batteries. *Nat. Energy* 1, 16113.
19. Wang, C., Wu, H., Chen, Z., McDowell, M.T., Cui, Y., and Bao, Z. (2013). Self-healing chemistry enables the stable operation of silicon microparticle anodes for high-energy lithium-ion batteries. *Nat. Chem.* 5, 1042–1048.
20. Sun, Y., Liu, N., and Cui, Y. (2016). Promises and challenges of nanomaterials for lithium-based rechargeable batteries. *Nat. Energy* 1, 16071.
21. Choi, N.S., Chen, Z., Freunberger, S.A., Ji, X., Sun, Y.K., Amine, K., Yushin, G., Nazar, L.F., Cho, J., and Bruce, P.G. (2012). Challenges facing lithium batteries and electrical double-layer capacitors. *Angew. Chem. Int. Ed.* 51, 9994–10024.
22. Goodenough, J.B., and Kim, Y. (2010). Challenges for rechargeable Li batteries. *Chem. Mater.* 22, 587–603.
23. Melot, B.C., and Tarascon, J.M. (2013). Design and preparation of materials for advanced electrochemical storage. *Acc. Chem. Res.* 46, 1226–1238.
24. Armand, M., and Tarascon, J.M. (2008). Building better batteries. *Nature* 451, 652–657.
25. Palacin, M.R. (2009). Recent advances in rechargeable battery materials: a chemist's perspective. *Chem. Soc. Rev.* 38, 2565–2575.
26. Van der Ven, A., Bhattacharya, J., and Belak, A.A. (2013). Understanding Li diffusion in Li-intercalation compounds. *Acc. Chem. Res.* 46, 1216–1225.
27. Whittingham, M.S. (2014). Ultimate limits to intercalation reactions for lithium batteries. *Chem. Rev.* 114, 11414–11443.
28. Obrovac, M.N., and Chevrier, V.L. (2014). Alloy negative electrodes for Li-ion batteries. *Chem. Rev.* 114, 11444–11502.
29. Croguennec, L., and Palacín, M.R. (2015). Recent achievements on inorganic electrode materials for lithium-ion batteries. *J. Am. Chem. Soc.* 137, 3140–3156.
30. Poizot, P., Laruelle, S., Gruegeon, S., Dupont, L., and Tarascon, J.M. (2000). Nano-sized transition-metal oxides as negative-electrode materials for lithium-ion batteries. *Nature* 407, 496–499.
31. Verma, P., Maire, P., and Novák, P. (2010). A review of the features and analyses of the solid electrolyte interphase in Li-ion batteries. *Electrochim. Acta* 55, 6332–6341.
32. Edström, K., Gustafsson, T., and Thomas, J.O. (2004). The cathode-electrolyte interface in the Li-ion battery. *Electrochim. Acta* 50, 397–403.
33. Gao, J., Shi, S.-Q., and Li, H. (2016). Brief overview of electrochemical potential in lithium ion batteries. *Chin. Phys. B* 25, 018210.
34. Hu, M., Pang, X., and Zhou, Z. (2013). Recent progress in high-voltage lithium ion batteries. *J. Power Sources* 237, 229–242.
35. Ceder, G. (2011). Opportunities and challenges for first-principles materials design and applications to Li battery materials. *MRS Bull.* 35, 693–701.
36. Toyoura, K., Koyama, Y., Kuwabara, A., Oba, F., and Tanaka, I. (2008). First-principles approach to chemical diffusion of lithium atoms in a graphite intercalation compound. *Phys. Rev. B* 78, 214303.
37. Bhattacharya, J., and Van der Ven, A. (2011). First-principles study of competing mechanisms of nondilute Li diffusion in spinel  $\text{Li}_x\text{TiS}_2$ . *Phys. Rev. B* 83, 144302.
38. Zhao, Y., Han, C., Yang, J., Su, J., Xu, X., Li, S., Xu, L., Fang, R., Jiang, H., Zou, X., et al. (2015). Stable alkali metal ion intercalation compounds as optimized metal oxide nanowire cathodes for lithium batteries. *Nano Lett.* 15, 2180–2185.
39. Kundu, D., Adams, B.D., Ort, V.D., Vajargah, S.H., and Nazar, L.F. (2016). A high-capacity and long-life aqueous rechargeable zinc battery using a metal oxide intercalation cathode. *Nat. Energy* 1, 16119.
40. An, Q., Xiong, F., Wei, Q., Sheng, J., He, L., Ma, D., Yao, Y., and Mai, L. (2015). Nanoflake-assembled hierarchical  $\text{Na}_3\text{V}_2(\text{PO}_4)_3/\text{C}$  microflowers: superior Li storage performance and insertion/extraction mechanism. *Adv. Energy Mater.* 5, 1401963.
41. Liang, Y., Yoo, H.D., Li, Y., Shuai, J., Calderon, H.A., Robles Hernandez, F.C., Grabow, L.C., and Yao, Y. (2015). Interlayer-expanded molybdenum disulfide nanocomposites for electrochemical magnesium storage. *Nano Lett.* 15, 2194–2202.
42. Wang, X., Niu, C., Meng, J., Hu, P., Xu, X., Wei, X., Zhou, L., Zhao, K., Luo, W., Yan, M., and Mai, L. (2015). Novel  $\text{K}_3\text{V}_2(\text{PO}_4)_3/\text{C}$  bundled nanowires as superior sodium-ion battery electrode with ultrahigh cycling stability. *Adv. Energy Mater.* 5, 1500716.
43. Wen, Y., He, K., Zhu, Y., Han, F., Xu, Y., Matsuda, I., Ishii, Y., Cumings, J., and Wang, C. (2014). Expanded graphite as superior anode for sodium-ion batteries. *Nat. Commun.* 5, 4033.
44. Yabuuchi, N., Kajiyama, M., Iwatate, J., Nishikawa, H., Hitomi, S., Okuyama, R., Usui, R., Yamada, Y., and Komaba, S. (2012). P2-type  $\text{Na}_x[\text{Fe}_{1/2}\text{Mn}_{1/2}]\text{O}_2$  made from earth-abundant elements for rechargeable Na batteries. *Nat. Mater.* 11, 512–517.
45. Tepavcevic, S., Xiong, H., Stamenovic, V.R., Zuo, X., Balasubramanian, M., Prakapenka, V.B., Johnson, C.S., and Rajh, T. (2012). Nanostructured bilayered vanadium oxide electrodes for rechargeable sodium-ion batteries. *ACS Nano* 6, 530–538.
46. Lee, J., Urban, A., Li, X., Su, D., Hautier, G., and Ceder, G. (2014). Unlocking the potential of cation-disordered oxides for rechargeable lithium batteries. *Science* 343, 519–522.
47. Liu, W., Oh, P., Liu, X., Myeong, S., Cho, W., and Cho, J. (2015). Countering voltage decay and capacity fading of lithium-rich cathode material at 60 °C by hybrid surface protection layers. *Adv. Energy Mater.* 5, 1500274.
48. Zhou, Y.N., Ma, J., Hu, E., Yu, X., Gu, L., Nam, K.W., Chen, L., Wang, Z., and Yang, X.Q. (2014). Tuning charge-discharge induced unit cell breathing in layer-structured cathode materials for lithium-ion batteries. *Nat. Commun.* 5, 5381.
49. Wang, Y., Yu, X., Xu, S., Bai, J., Xiao, R., Hu, Y.S., Li, H., Yang, X.Q., Chen, L., and Huang, X. (2013). A zero-strain layered metal oxide as the negative electrode for long-life sodium-ion batteries. *Nat. Commun.* 4, 2365.
50. Kim, H., Lee, S., Cho, H., Kim, J., Lee, J., Park, S., Joo, S.H., Kim, S.H., Cho, Y.G., Song, H.K., et al. (2016). Enhancing interfacial bonding between anisotropically oriented grains using a glue-nanofiller for advanced Li-ion battery cathode. *Adv. Mater.* 28, 4705–4712.
51. Wang, B., Al Abdulla, W., Wang, D., and Zhao, X.S. (2015). A three-dimensional porous  $\text{LiFePO}_4$  cathode material modified with a nitrogen-doped graphene aerogel for high-power lithium ion batteries. *Energy Environ. Sci.* 8, 869–875.
52. Wang, Y., Liu, J., Lee, B., Qiao, R., Yang, Z., Xu, S., Yu, X., Gu, L., Hu, Y.-S., Yang, W., et al. (2015). Ti-substituted tunnel-type  $\text{Na}_{0.44}\text{MnO}_2$  oxide as a negative electrode for aqueous sodium-ion batteries. *Nat. Commun.* 6, 6401.
53. Li, Z., Chernova, N.A., Feng, J., Upreti, S., Omenya, F., and Whittingham, M.S. (2012). Stability and rate capability of Al substituted lithium-rich high-manganese content oxide materials for Li-ion batteries. *J. Electrochem. Soc.* 159, A116–A120.
54. Paoletta, A., Turner, S., Bertoni, G., Hovington, P., Flacau, R., Boyer, C., Feng, Z., Colombo, M., Marras, S., Prato, M., et al. (2016). Accelerated removal of Fe-antisite defects while nanosizing hydrothermal  $\text{LiFePO}_4$  with  $\text{Ca}^{2+}$ . *Nano Lett.* 16, 2692–2697.
55. Zhang, P., Wang, Y., Lin, M., Zhang, D., Ren, X., and Yuan, Q. (2012). Doping effect of  $\text{Nb}^{5+}$  on the microstructure and defects of  $\text{LiFePO}_4$ . *J. Electrochem. Soc.* 159, A402–A409.
56. Liu, H., Cao, Q., Fu, L.J., Li, C., Wu, Y.P., and Wu, H.Q. (2006). Doping effects of zinc on  $\text{LiFePO}_4$  cathode material for lithium ion batteries. *Electrochim. Commun.* 8, 1553–1557.
57. Zhang, L.-L., Liang, G., Ignatov, A., Croft, M.C., Xiong, X.-Q., Hung, I.M., Huang, Y.-H., Hu, X.-L., Zhang, W.-X., and Peng, Y.-L. (2011).

- Effect of vanadium incorporation on electrochemical performance of LiFePO<sub>4</sub> for lithium-ion batteries. *J. Phys. Chem. C* 115, 13520–13527.
58. Shi, S., Liu, L., Ouyang, C., Wang, D.-s., Wang, Z., Chen, L., and Huang, X. (2003). Enhancement of electronic conductivity of LiFePO<sub>4</sub> by Cr doping and its identification by first-principles calculations. *Phys. Rev. B* 68, 195108.
59. Omenya, F., Wen, B., Fang, J., Zhang, R., Wang, Q., Chernova, N.A., Schneider-Haefner, J., Cosandey, F., and Whittingham, M.S. (2015). Mg substitution clarifies the reaction mechanism of olivine LiFePO<sub>4</sub>. *Adv. Energy Mater.* 5, 1401204.
60. Guo, S., Liu, P., Yu, H., Zhu, Y., Chen, M., Ishida, M., and Zhou, H. (2015). A layered P2- and O3-type composite as a high-energy cathode for rechargeable sodium-ion batteries. *Angew. Chem. Int. Ed.* 54, 5894–5899.
61. Sun, Y.-K., Myung, S.-T., Park, B.-C., Prakash, J., Belharouak, I., and Amine, K. (2009). High-energy cathode material for long-life and safe lithium batteries. *Nat. Mater.* 8, 320–324.
62. Kim, S., Cho, W., Zhang, X., Oshima, Y., and Choi, J.W. (2016). A stable lithium-rich surface structure for lithium-rich layered cathode materials. *Nat. Commun.* 7, 13598.
63. Hwang, J.Y., Oh, S.M., Myung, S.T., Chung, K.Y., Belharouak, I., and Sun, Y.K. (2015). Radially aligned hierarchical columnar structure as a cathode material for high energy density sodium-ion batteries. *Nat. Commun.* 6, 6865.
64. Niu, C., Liu, X., Meng, J., Xu, L., Yan, M., Wang, X., Zhang, G., Liu, Z., Xu, X., and Mai, L. (2016). Three dimensional V<sub>2</sub>O<sub>5</sub>/NaV<sub>6</sub>O<sub>15</sub> hierarchical heterostructures: controlled synthesis and synergistic effect investigated by *in situ* X-ray diffraction. *Nano Energy* 27, 147–156.
65. Reddy, M.V., Subba Rao, G.V., and Chowdari, B.V.R. (2013). Metal oxides and oxysalts as anode materials for Li ion batteries. *Chem. Rev.* 113, 5364–5457.
66. Kim, D.W., Ko, Y.D., Park, J.G., and Kim, B.K. (2007). Formation of lithium-driven active/inactive nanocomposite electrodes based on Ca<sub>2</sub>Co<sub>3</sub>O<sub>9</sub> nanoplates. *Angew. Chem. Int. Ed.* 46, 6654–6657.
67. Chae, S., Ko, M., Park, S., Kim, N., Ma, J., and Cho, J. (2016). Micron-sized Fe–Cu–Si ternary composite anodes for high energy Li-ion batteries. *Energy Environ. Sci.* 9, 1251–1257.
68. Liu, J., Wen, Y., van Aken, P.A., Maier, J., and Yu, Y. (2014). Facile synthesis of highly porous Ni–Sn intermetallic microcages with excellent electrochemical performance for lithium and sodium storage. *Nano Lett.* 14, 6387–6392.
69. Lin, L., Xu, X., Chu, C., Majeed, M.K., and Yang, J. (2016). Mesoporous amorphous silicon: a simple synthesis of a high-rate and long-life anode material for lithium-ion batteries. *Angew. Chem. Int. Ed.* 55, 14063–14066.
70. Wang, X., Gu, W., Lee, J.T., Nitta, N., Benson, J., Magasinski, A., Schauer, M.W., and Yushin, G. (2015). Carbon nanotube–CoF<sub>2</sub> multifunctional cathode for lithium ion batteries: effect of electrolyte on cycle stability. *Small* 11, 5164–5173.
71. Wang, F., Kim, S.-W., Seo, D.-H., Kang, K., Wang, L., Su, D., Vajo, J.J., Wang, J., and Graetz, J. (2015). Ternary metal fluorides as high-energy cathodes with low cycling hysteresis. *Nat. Commun.* 6, 6668.
72. Wu, H., Yu, G., Pan, L., Liu, N., McDowell, M.T., Bao, Z., and Cui, Y. (2013). Stable Li-ion battery anodes by *in-situ* polymerization of conducting hydrogel to conformally coat silicon nanoparticles. *Nat. Commun.* 4, 1943.
73. Shi, Y., Zhang, J., Pan, L., Shi, Y., and Yu, G. (2016). Energy gels: a bio-inspired material platform for advanced energy applications. *Nano Today* 11, 738–762.
74. Shi, Y., Zhou, X., Zhang, J., Bruck, A.M., Bond, A.C., Marschilok, A.C., Takeuchi, K.J., Takeuchi, E.S., and Yu, G. (2017). Nanostructured conductive polymer gels as a general framework material to improve electrochemical performance of cathode materials in Li-ion batteries. *Nano Lett.* 17, 1906–1914.
75. Shi, Y., Zhang, J., Bruck, A.M., Zhang, Y., Li, J., Stach, E.A., Takeuchi, K.J., Marschilok, A.C., Takeuchi, E.S., and Yu, G. (2017). A tunable 3D nanostructured conductive gel framework electrode for high-performance lithium ion batteries. *Adv. Mater.* <https://doi.org/10.1002/adma.201603922>.
76. Jin, Y., Li, S., Kushima, A., Zheng, X., Sun, Y., Xie, J., Sun, J., Xue, W., Zhou, G., Wu, J., et al. (2017). Self-healing SEI enables full-cell cycling of a silicon-majority anode with a coulombic efficiency exceeding 99.9%. *Energy Environ. Sci.* 10, 580–592.
77. Zheng, G., Lee, S.W., Liang, Z., Lee, H.W., Yan, K., Yao, H., Wang, H., Li, W., Chu, S., and Cui, Y. (2014). Interconnected hollow carbon nanospheres for stable lithium metal anodes. *Nat. Nanotechnol.* 9, 618–623.
78. Bresser, D., Passerini, S., and Scrosati, B. (2016). Leveraging valuable synergies by combining alloying and conversion for lithium-ion anodes. *Energy Environ. Sci.* 9, 3348–3367.
79. Jiang, Y., Li, Y., Zhou, P., Lan, Z., Lu, Y., Wu, C., and Yan, M. (2017). Ultrafast, highly reversible, and cycle-stable lithium storage boosted by pseudocapacitance in Sn-based alloying anodes. *Adv. Mater.* <https://doi.org/10.1002/adma.20160499>.
80. Hu, R., Ouyang, Y., Liang, T., Wang, H., Liu, J., Chen, J., Yang, C., Yang, L., and Zhu, M. (2017). Stabilizing the nanostructure of SnO<sub>2</sub> anodes by transition metals: a route to achieve high initial coulombic efficiency and stable capacities for lithium storage. *Adv. Mater.* 29, 1605006, <https://doi.org/10.1002/adma.201605006>.
81. Liu, W., Oh, P., Liu, X., Lee, M.J., Cho, W., Chae, S., Kim, Y., and Cho, J. (2015). Nickel-rich layered lithium transition-metal oxide for high-energy lithium-ion batteries. *Angew. Chem. Int. Ed.* 54, 4440–4457.
82. Zheng, J., Gu, M., Genc, A., Xiao, J., Xu, P., Chen, X., Zhu, Z., Zhao, W., Pullan, L., Wang, C., and Zhang, J.G. (2014). Mitigating voltage fade in cathode materials by improving the atomic level uniformity of elemental distribution. *Nano Lett.* 14, 2628–2635.
83. Kim, H., Kim, M.G., Jeong, H.Y., Nam, H., and Cho, J. (2015). A new coating method for alleviating surface degradation of LiNi<sub>0.4</sub>Co<sub>0.2</sub>Mn<sub>0.2</sub>O<sub>2</sub> cathode material: nanoscale surface treatment of primary particles. *Nano Lett.* 15, 2111–2119.
84. Oh, P., Ko, M., Myeong, S., Kim, Y., and Cho, J. (2014). A novel surface treatment method and new insight into discharge voltage deterioration for high-performance 0.4Li<sub>2</sub>MnO<sub>3</sub>–0.6LiNi<sub>1/3</sub>Co<sub>1/3</sub>Mn<sub>1/3</sub>O<sub>2</sub> cathode materials. *Adv. Energy Mater.* 4, 1400631.
85. Bian, X., Fu, Q., Bie, X., Yang, P., Qiu, H., Pang, Q., Chen, G., Du, F., and Wei, Y. (2015). Improved electrochemical performance and thermal stability of Li-excess Li<sub>1.18</sub>Co<sub>0.15</sub>Ni<sub>0.15</sub>Mn<sub>0.52</sub>O<sub>2</sub> cathode material by Li<sub>3</sub>PO<sub>4</sub> surface coating. *Electrochim. Acta* 174, 875–884.
86. Sun, Y.K., Lee, M.J., Yoon, C.S., Hassoun, J., Amine, K., and Scrosati, B. (2012). The role of AlF<sub>3</sub> coatings in improving electrochemical cycling of Li-enriched nickel-manganese oxide electrodes for Li-ion batteries. *Adv. Mater.* 24, 1192–1196.
87. Yang, J., and Xia, Y. (2016). Suppressing the phase transition of the layered Ni-rich oxide cathode during high-voltage cycling by introducing low-content Li<sub>2</sub>MnO<sub>3</sub>. *ACS Appl. Mater. Inter.* 8, 1297–1308.
88. Yu, D.Y.W., Yanagida, K., and Nakamura, H. (2010). Surface modification of Li-excess Mn-based cathode materials. *J. Electrochem. Soc.* 157, A1177–A1182.
89. Lee, M.-J., Noh, M., Park, M.-H., Jo, M., Kim, H., Nam, H., and Cho, J. (2015). The role of nanoscale-range vanadium treatment in LiNi<sub>0.8</sub>Co<sub>0.15</sub>Al<sub>0.05</sub>O<sub>2</sub> cathode materials for Li-ion batteries at elevated temperatures. *J. Mater. Chem. A* 3, 13453–13460.
90. Li, L., Chen, Z., Zhang, Q., Xu, M., Zhou, X., Zhu, H., and Zhang, K. (2015). A hydrolysis-hydrothermal route for the synthesis of ultrathin LiAlO<sub>2</sub>-inlaid LiNi<sub>0.5</sub>Co<sub>0.2</sub>Mn<sub>0.3</sub>O<sub>2</sub> as a high-performance cathode material for lithium ion batteries. *J. Mater. Chem. A* 3, 894–904.
91. Lee, K.T., Ramesh, T.N., Nan, F., Botton, G., and Nazar, L.F. (2011). Topochemical synthesis of sodium metal phosphate olivines for sodium-ion batteries. *Chem. Mater.* 23, 3593–3600.
92. Mukhopadhyay, A., and Sheldon, B.W. (2014). Deformation and stress in electrode materials for Li-ion batteries. *Prog. Mater. Sci.* 63, 58–116.
93. Yan, P., Zheng, J., Gu, M., Xiao, J., Zhang, J.G., and Wang, C.M. (2017). Intragranular cracking as a critical barrier for high-voltage usage of layer-structured cathode for lithium-ion batteries. *Nat. Commun.* 8, 14101.
94. Huang, Z.-D., Liu, X.-M., Oh, S.-W., Zhang, B., Ma, P.-C., and Kim, J.-K. (2011). Microscopically porous, interconnected

- single crystal  $\text{LiNi}_{1/3}\text{Co}_{1/3}\text{Mn}_{1/3}\text{O}_2$  cathode material for lithium ion batteries. *J. Mater. Chem.* 21, 10777–10784.
95. Sun, C., Rajasekharan, S., Goodenough, J.B., and Zhou, F. (2011). Monodisperse porous  $\text{LiFePO}_4$  microspheres for a high power Li-ion battery cathode. *J. Am. Chem. Soc.* 133, 2132–2135.
96. Li, B., Yan, H., Ma, J., Yu, P., Xia, D., Huang, W., Chu, W., and Wu, Z. (2014). Manipulating the electronic structure of Li-rich manganese-based oxide using polyanions: towards better electrochemical performance. *Adv. Funct. Mater.* 24, 5112–5118.
97. Zheng, Z., Guo, X.-D., Zhong, Y.-J., Hua, W.-B., Shen, C.-H., Chou, S.-L., and Yang, X.-S. (2016). Host structural stabilization of  $\text{Li}_{1.23}\text{Mn}_{0.615}\text{Ni}_{0.154}\text{O}_2$  through K-doping attempt: toward superior electrochemical performances. *Electrochim. Acta* 188, 336–343.
98. Kim, J., Cho, H., Jeong, H.Y., Ma, H., Lee, J., Hwang, J., Park, M., and Cho, J. (2017). Self-induced concentration gradient in nickel-rich cathodes by sacrificial polymeric bead clusters for high-energy lithium-ion batteries. *Adv. Energy Mater.* 7, 1602559.
99. Lee, J.H., Yoon, C.S., Hwang, J.-Y., Kim, S.-J., Maglia, F., Lamp, P., Myung, S.-T., and Sun, Y.-K. (2016). High-energy-density lithium-ion battery using a carbon-nanotube–Si composite anode and a compositionally graded  $\text{Li}[\text{Ni}_{0.85}\text{Co}_{0.05}\text{Mn}_{0.10}]\text{O}_2$  cathode. *Energy Environ. Sci.* 9, 2152–2158.
100. Zheng, F., Yang, C., Xiong, X., Xiong, J., Hu, R., Chen, Y., and Liu, M. (2015). Nanoscale surface modification of lithium-rich layered-oxide composite cathodes for suppressing voltage fade. *Angew. Chem. Int. Ed.* 54, 13058–13062.
101. Kim, U.-H., Lee, E.-J., Yoon, C.S., Myung, S.-T., and Sun, Y.-K. (2016). Compositionally graded cathode material with long-term cycling stability for electric vehicles application. *Adv. Energy Mater.* 6, 1601417.
102. Wang, F., Robert, R., Chernova, N.A., Pereira, N., Omenya, F., Badway, F., Hua, X., Ruotolo, M., Zhang, R., Wu, L., et al. (2011). Conversion reaction mechanisms in lithium ion batteries: study of the binary metal fluoride electrodes. *J. Am. Chem. Soc.* 133, 18828–18836.
103. Son, I.H., Hwan Park, J., Kwon, S., Park, S., Rummeli, M.H., Bachmatiuk, A., Song, H.J., Ku, J., Choi, J.W., Choi, J.M., et al. (2015). Silicon carbide-free graphene growth on silicon for lithium-ion battery with high volumetric energy density. *Nat. Commun.* 6, 7393.
104. Lin, D., Liu, Y., and Cui, Y. (2017). Reviving the lithium metal anode for high-energy batteries. *Nat. Nanotechnol.* 12, 194–206.
105. Lin, D., Zhao, J., Sun, J., Yao, H., Liu, Y., Yan, K., and Cui, Y. (2017). Three-dimensional stable lithium metal anode with nanoscale lithium islands embedded in ionically conductive solid matrix. *Proc. Natl. Acad. Sci. USA* 114, 4613–4618.
106. Markevich, E., Salitra, G., Chesneau, F., Schmidt, M., and Aurbach, D. (2017). Very stable lithium metal stripping-plating at a high rate and high areal capacity in fluoroethylene carbonate-based organic electrolyte solution. *ACS Energy Lett.* 2, 1321–1326.
107. Mai, L., Dong, Y., Xu, L., and Han, C. (2010). Single nanowire electrochemical devices. *Nano Lett.* 10, 4273–4278.
108. Huang, J.Y., Zhong, L., Wang, C.M., Sullivan, J.P., Xu, W., Zhang, L.Q., Mao, S.X., Hudak, N.S., Liu, X.H., Subramanian, A., et al. (2010). In situ observation of the electrochemical lithiation of a single  $\text{SnO}_2$  nanowire electrode. *Science* 330, 1515–1520.
109. Yu, X., Lyu, Y., Gu, L., Wu, H., Bak, S.-M., Zhou, Y., Amine, K., Ehrlich, S.N., Li, H., Nam, K.-W., and Yang, X.-Q. (2014). Understanding the rate capability of high-energy-density Li-rich layered  $\text{Li}_{1.2}\text{Ni}_{0.15}\text{Co}_{0.1}\text{Mn}_{0.55}\text{O}_2$  cathode materials. *Adv. Energy Mater.* 4, 1300950.
110. Liu, H., Strobridge, F.C., Borkiewicz, O.J., Wiaderek, K.M., Chapman, K.W., Chupas, P.J., and Grey, C.P. (2014). Capturing metastable structures during high-rate cycling of  $\text{LiFePO}_4$  nanoparticle electrodes. *Science* 344, 1252817.
111. Chevrier, V.L., Ong, S.P., Armiento, R., Chan, M.K.Y., and Ceder, G. (2010). Hybrid density functional calculations of redox potentials and formation energies of transition metal compounds. *Phys. Rev. B* 82, 075122.
112. Clark, J.M., Nishimura, S., Yamada, A., and Islam, M.S. (2012). High-voltage pyrophosphate cathode: insights into local structure and lithium-diffusion pathways. *Angew. Chem. Int. Ed.* 51, 13149–13153.
113. Kim, H., Kim, D.J., Seo, D.-H., Yeom, M.S., Kang, K., Kim, D.K., and Jung, Y. (2012). Ab initio study of the sodium intercalation and intermediate phases in  $\text{Na}_{0.44}\text{MnO}_2$  for sodium-ion battery. *Chem. Mater.* 24, 1205–1211.
114. Sun, Y., Zhao, L., Pan, H., Lu, X., Gu, L., Hu, Y.S., Li, H., Armand, M., Ikuhara, Y., Chen, L., and Huang, X. (2013). Direct atomic-scale confirmation of three-phase storage mechanism in  $\text{Li}_4\text{Ti}_5\text{O}_{12}$  anodes for room-temperature sodium-ion batteries. *Nat. Commun.* 4, 1870.
115. Ma, X., Luo, W., Yan, M., He, L., and Mai, L. (2016). In situ characterization of electrochemical processes in one dimensional nanomaterials for energy storage devices. *Nano Energy* 24, 165–188.
116. Hovington, P., Lagace, M., Guerfi, A., Bouchard, P., Mauger, A., Julien, C.M., Armand, M., and Zaghib, K. (2015). New lithium metal polymer solid state battery for an ultrahigh energy: nano C- $\text{LiFePO}_4$  versus nano  $\text{Li}_{1.2}\text{V}_3\text{O}_8$ . *Nano Lett.* 15, 2671–2678.
117. Islam, M.S., and Fisher, C.A.J. (2014). Lithium and sodium battery cathode materials: computational insights into voltage, diffusion and nanostructural properties. *Chem. Soc. Rev.* 43, 185–204.
118. Song, Z., and Zhou, H. (2013). Towards sustainable and versatile energy storage devices: an overview of organic electrode materials. *Energy Environ. Sci.* 6, 2280–2301.